RL-TR-96-43
Final Technical Report
March 1996

DEVELOPMENT OF METHODOLOGIES FOR ELECTROMAGNETIC SUSCEPTIBILITY EVALUATION

CALSPAN-UB Research Center

Dr. John P. Quine

APPROVED FOR PUBLIC RELEASE; DISTRIBUTION UNLIMITED.

Rome Laboratory
Air Force Materiel Command
Rome, New York

This report has been reviewed by the Rome Laboratory Public Affairs Office (PA) and is releasable to the National Technical Information Service (NTIS). At NTIS, it will be releasable to the general public, including foreign nations.

RL-TR- 96-43 has been reviewed and is approved for publication.

APPROVED: Anthony J Pesta

ANTHONY J. PESTA
Project Engineer

FOR THE COMMANDER: John J. Bart

JOHN J. BART
Chief Scientist, Reliability Sciences
Electromagnetics & Reliability Directorate

If your address has changed or if you wish to be removed from the Rome Laboratory mailing list, or if the addressee is no longer employed by your organization, please notify Rome Laboratory/ (ERST), Rome NY 13441. This will assist us in maintaining a current mailing list.

Do not return copies of this report unless contractual obligations or notices on a specific document require that it be returned.

REPORT DOCUMENTATION PAGE

Form Approved
OMB No. 0704-0188

1. AGENCY USE ONLY (Leave Blank)	2. REPORT DATE	3. REPORT TYPE AND DATES COVERED
	March 1996	Final ----

4. TITLE AND SUBTITLE

DEVELOPMENT OF METHODOLOGIES FOR ELECTROMAGNETIC SUSCEPTIBILITY EVALUATION

5. FUNDING NUMBERS

C - F30602-88-D-0026, Task 57
PE - 62702F
PR - 2338
TA - 03
WU - P4

6. AUTHOR(S)

Dr. John P. Quine

7. PERFORMING ORGANIZATION NAME(S) AND ADDRESS(ES)

CALSPAN-UB Research Center
P.O. Box 400
Buffalo NY 14225

8. PERFORMING ORGANIZATION REPORT NUMBER

N/A

9. SPONSORING/MONITORING AGENCY NAME(S) AND ADDRESS(ES)

Rome Laboratory/ERST
525 Brooks Rd
Rome NY 13441-4505

10. SPONSORING/MONITORING AGENCY REPORT NUMBER

RL-TR-96-43

11. SUPPLEMENTARY NOTES

Rome Laboratory Project Engineer: Anthony J. Pesta/ESRT/(315) 330-7642

12a. DISTRIBUTION/AVAILABILITY STATEMENT

Approved for public release; distribution unlimited.

12b. DISTRIBUTION CODE

13. ABSTRACT (Maximum 200 words)

The contractor investigated the use of frequency modulated (FM), band limited noise signals and other applicable techniques to increase the speed of making coupling and shielding effectiveness measurements in reverberation chambers; developed the most promising techniques and analytical approaches for usable methodologies to predict the effect of electromagnetic fields on the operational performance of electronic systems; and developed and investigated new assessment techniques using reverberation chambers that will quickly determine the total amount of energy absorbed and/or reflected by electronic equipment as a function of frequency.

14. SUBJECT TERMS

Reverberation chambers, Electromagnetic fields, Shielding enclosures

15. NUMBER OF PAGES

60

16. PRICE CODE

17. SECURITY CLASSIFICATION OF REPORT	18. SECURITY CLASSIFICATION OF THIS PAGE	19. SECURITY CLASSIFICATION OF ABSTRACT	20. LIMITATION OF ABSTRACT
UNCLASSIFIED	UNCLASSIFIED	UNCLASSIFIED	UL

TABLE OF CONTENTS

1.0 INTRODUCTION

This work was performed for Rome Laboratories, Rome Air Force Base, NY under prime contract F30602-88D-0026 with CALSPANN/UB Research Center and subcontract C/UB-63:D.O. No. 0057. This report was written by Dr. John P. Quine, Consultant for Rome Laboratories with technical participation and contributions by John P. Streeter, Edward Surowiec, Kenneth E. Larsen (formerly) of the Rome Research Corporation and Anthony J. Pesta of the Rome Laboratories.

1.1 Statement of Work

The Contractor shall investigate the use of Frequency Modulated (FM), Band limited noise signals and other applicable techniques to increase the speed of making coupling and shielding effectiveness measurements in reverberation chambers. Develop the most promising techniques and analytical approaches into usable methodologies to predict the effect of electromagnetic fields on the operational performance of electronic systems. Develop and investigate new assessment techniques using reverberation chambers, that will quickly determine the total amount of energy absorbed and/or reflected by electronic equipment as a function of frequency.

1.2 Program Objectives

1) Develop methodologies leading to increased data speed in reverberation chamber measurements.

2) Develop methodologies for measuring total power absorbed by electronic modules located inside shielded enclosures.

3) Develop the most promising techniques into usable methodologies.

Overview

The application of reverberation chambers for susceptibility evaluation was the principal objective of this study. Research effort is currently being directed towards increasing the rate at which measurements can be made, and mode stirring by fast electronic modulation of the source frequency is a promising approach. Electromagnetic analysis of a reverberation chamber with a mechanical mode stirrer would present a formidable, if not an intractable task. However, a reverberation chamber with no mechanical mode stirrer can be realistically modeled as an unperturbed empty rectangular cavity, the analysis of which can be accomplished with a reasonable effort. A computer program was therefore developed for calculating the fields inside a rectangular enclosure, and is described in Section 2. The enclosure can be as large as the reverberation chamber at Rome Laboratories (3.69 x 5.18 x 9.78 meters). Much smaller shielding enclosures can also be studied. It was felt that such a program would permit a detailed study of reverberation chamber and shielding enclosure characteristics that would otherwise be more difficult to determine experimentally.

The Black-Hole Principle is discussed in Section 3, and is employed as a basis for establishing the lowest frequency for operation of an enclosure as a reverberation chamber. The frequency ranges for single isolated resonant modes, and for overlapping modes are also defined. These three frequency ranges are related to the number of modes that can exist within the bandwidths determined by internal dissipation through the Q-factor. An effective aperture for wall losses is also derived in Section 3, and is employed to determine the reduction in chamber Q-value due to an opening in the wall of the chamber.

Experimental results obtained with an available 30 -inch cubic enclosure are presented in Section 4.0. The purpose was to show that it is feasible to measure the total power that enters (and is dissipated) inside an enclosure from a measurement of the enclosure Q and the internal fields on the walls of the enclosure. Furthermore, it was desired to show that this can be accomplished with simple "homemade" small B-dot or D-dot surface probes that can be inserted from outside the enclosure through small (0.25" diameter) holes in the enclosure wall. It was found that calculated power was within a few dB of the actual measured input power, and that the probe output power readings were stable and repeatable for both B-dot and D-dot probes. A simple method for accurately calibrating these probes is also described. Based on these favorable results, it may be possible to devise simple measurement methodologies employing these insertable probes. Two examples of such methodologies are described in Section 5.0

Section 5.0 also presents methodologies for measuring leakage transmission through gaskets and highly attenuating cover panels. It is shown that because of non-uniformities in material, construction or installation, the leakage transmission can vary along the length of the gasket or over the area of the cover panel. This causes the leakage wavefront and radiation pattern on the output side of the gasket and panel to be highly distorted and unpredictable. It is therefore concluded that in order to measure the total leakage power radiated in all directions, the gasket or panel should radiate into a large reverberation chamber. In the case of gaskets, it is also shown that the low frequency concept of Transfer Impedance fails at microwave frequencies (gasket length greater than about one-half wavelength), and that characterization of a gasket in terms of effective area per unit length is more meaningful. The similarity between gasket and panel leakage is emphasized. Thus, the gasket acts as a one-dimensional line-source antenna and the panel as a two-dimensional aperture antenna. On this basis, both can be appropriately characterized by leakage transmission areas, and measurement methodologies can be similar for both.

2.0 COMPUTER PROGRAM FOR CALCULATING THE FIELDS INSIDE A LARGE RECTANGULAR METAL ENCLOSURE

2.1 Description of the Program

The application of reverberation chambers for susceptibility evaluation was the principal objective of this study. Research effort is currently being directed towards increasing the rate at which measurements can be made, and mode stirring by fast electronic modulation of the source frequency is a promising approach. Electromagnetic analysis of a reverberation chamber with a mechanical mode stirrer would present a formidable, if not an intractable task. However, a reverberation chamber with no mechanical mode stirrer can be realistically modeled as an unperturbed empty rectangular cavity, the analysis of which can be accomplished with a reasonable effort. A computer program was therefore developed for calculating the fields inside a rectangular enclosure having dimensions of the same order as the large chamber at Rome Laboratories (3.69 x 5.18 x 9.78 meters). It was felt that such a program would permit a detailed study of chamber characteristics that would otherwise be more difficult to determine experimentally.

Although analysis of a practical rectangular enclosure is relatively less difficult with no mode stirrer, there still remain problems associated with the finite conductivity of the enclosure walls. For example, it would be desirable to expand the fields inside the enclosure in terms of the relatively simple TE_{mn} and TM_{mn} modes associated with an infinitely long rectangular waveguide, the enclosure being considered as a length of rectangular waveguide shorted at both ends, and excited by an external incident field through a hole at one end, as shown in the inset in Figure (2.1). These modes were originally derived for a rectangular waveguide with infinite wall conductivity , but with finite wall conductivity, they become coupled and are no longer an orthogonal set of modes. Therefore, if the conductivity of the waveguide walls is not infinite, these simple modes cannot be used to expand the fields in a Fourier modal analysis.

Rigorous account of the effects of modal coupling for degenerate TE_{mn}, TM_{mn} mode pairs [1] would significantly increase the analytical complexity and the required computer time. It should be noted, however, that the coupling due to finite wall conductivity is exactly zero for m or $n = 0$, and for a square waveguide cross-section. On this basis, it may be acceptable to neglect the coupling for cross-sections that are roughly square. Furthermore, it should also be noted that neglecting the coupling due to finite wall conductivity is mathematically equivalent to the assumption that the losses in the enclosure are due entirely to dielectric losses in the gas that fills the volume of the enclosure. With dielectric losses only and infinitely conducting walls, there are no modal coupling effects and the simple rectangular waveguide TE_{mn} and TM_{mn} modes are an orthogonal set of modes that can be employed to expand the fields in the enclosure. This is the approach that was adopted for the present program. It is felt that a high-Q cavity with only uniform wall losses cannot be readily distinguished from a cavity with only uniform dielectric

losses. Therefore, under these conditions, physical characteristics such as internal field distributions, buildup time, and autocorrelation widths are expected to be nearly alike for a specified Q-value. This assumes that wall losses are uniformly distributed over the internal surfaces of the enclosure. If significant wall losses are contributed by discrete discontinuities such as holes and seams along the wall surfaces, then wall losses may not be the same in detail to losses due to uniform dielectric losses, but may be similar on an average basis.

The inset in Figure (2.1) shows an enclosure comprised of a rectangular waveguide with shorting planes at each end. The enclosure has dimensions A, B, C, and is excited through a round hole of diameter D located at coordinates XH,YH on the end wall at Z = 0. Hole diameter, D is assumed to be small relative to the free-space wavelength. An incident H-field component parallel to the end wall creates a magnetic dipole with coordinates also equal to XH,YH on the inside surface of the end wall. The incident E-field component normal to the end wall creates an electric dipole on the inside surface (which is zero for normal incidence). Therefore, considering only nearly normal incidence, the fields inside the enclosure result mostly from the magnetic dipole caused by the parallel component of the incident H-field.

In general, the magnetic (and electric) dipoles excited inside the enclosure are related to the incident fields through the hole polarizeabilities [1], [2]. The dipole in turn excites each of the modes (e.g., TE_{mn}, TM_{mn}) that are employed as the orthogonal (uncoupled) set of modes.

As discussed above, a rectangular enclosure with infinitely conducting walls and only dielectric losses can be analyzed rigorously with the rectangular waveguide TE_{mn} and TM_{mn} modes. However, since these are degenerate mode pairs if m and n are the same as p and q, the degenerate pair can also be treated as a single mode normalized with unit power shared between the two component modes. Two orthogonally polarized single modes comprised of combinations of the TE_{mn}, TM_{mn} degenerate mode pair are called LSE_{mn} (or an LSM_{mn} mode) [1]. It can be shown that an incident H-field with only an x-component leaks through the round hole and excites only a magnetic dipole which in turn excites an E-field inside the enclosure which has only x and z components, x and y being transverse, and z axial (see Fig. 2.1). On the other hand, an incident H-field with only a y-component excites only x and z-components of E-field inside the enclosure. The modes with only Ey and Ez can be designated as $LSEY_{mn}$ modes, and the modes with only Ex and Ez as $LSEX_{mn}$ modes. The term LSE stands for longitudinal section E-field along either the y-z or x-z planes, and similarly for the LSM modes [1].

Under the above conditions, the $LSEY_{mn}$ and $LSEX_{mn}$ modes are also appropriate normal modes. The fields of these modes were derived as combinations of TE_{mn} and TM_{mn} modes which yield $E_x = 0$ for $LSEY_{mn}$ and $E_y = 0$ for $LSEX_{mn}$. The required component TE_{mn} and TM_{mn} modal powers were determined in this way and the sum representing the normalized LSEX or LSEY mode power was set equal to unity. The fields of the LSEX and LSEY modes were

obtained by summing the fields of the component TE_{mn} and TM_{mn} modes. Calculations were made using TE_{mn}, TM_{mn} modes in the field expansions, and also using $LSEX_{mn}$ and $LSEY_{mn}$ modes. The results with both sets of modes were the same, indicating that the equations derived for the modal power normalizations were correct. The program accuracy was also checked by calculating the values of the fields transmitted into the enclosure through the hole at one end (z = 0) as the enclosure length C was increased to large values. These fields were compared to the fields calculated for an infinitely long waveguide with matched termination, and were found to agree. This check indicated that the equations for modal resonance inside the enclosure were correct. The total power transmitted past the transverse plane at z = 0 was calculated by summing the power transmitted by each propagating mode. This power was typically 2 or 3 dB greater than the dissipated power associated with the Q and the magnetic field energy density stored in the volume of the enclosure. The energy density was calculated by averaging the square of the magnetic field over a 24-point array. The lack of complete agreement between the two power calculations results mainly from power dissipated near the dipole source at z = 0 by propagating modes that are close to cutoff. All modes were included in the power summation for which F was greater than 1.005 FC where F is applied and FC is the cutoff frequency. As discussed in Section 3.3, the program was also checked by comparing the total number of modes employed in the modal expansion with the value of N calculated from Eq. (3.2.6). The results of these comparisons indicate that Eq. (3.2.6) provides an upper bound which is typically to 20-30 percent high. Based on the several checks, it is believed that the computer calculations are accurate.

2.2 Calculated Internal Fields

Figure (2.1) shows representative calculations for an enclosure having the dimensions of the Rome Laboratories Chamber, but with no more stirrer present. The program allows the fields to be calculated at any number of field points arbitrarily located within the enclosure. For the calculations in the report, however, the field points were located in a planar array of uniformly spaced points as shown in Figure (2.2) and in the inset in Figure (2.3). The array is centered symmetrically in the transverse (x-y) plane and is normal to the z-axis. The data in Figure (2.1) show that the normalized average internal H-field magnitude HINT given by the square root of the sum of the squares of the x, y and z components remains within a range of about 1.8 dB as the array is moved axially from z = 0.45C to z = C. The H-fields are normalized relative to the incident H-field, HINC. The square of the normalized value therefore represents the inverse shielding effectiveness given by Eq. (3.2.4). The data in Figure (2.3) which apply for z = 0.7C show that much higher variations in H-field can occur from point-to-point within the array.

The ratio of magnitudes of the E and H-fields are also shown (in parenthesis) in Figure (2.3). As expected, values both higher and lower than 377 ohms occur at points of low and high H-fields, respectively. Note, however, that higher than 377 ohms is also obtained at two points

where the H-field has a relatively high value. Figure 2.4 for z = c (on the wall) shows somewhat higher peak and average values.

The average normalized value of the H-field magnitudes in Figure (2.1) is 0.329 x 10^{-3}, and corresponds to a shielding effectiveness of 69.66 dB due to leakage through the 0.200" diameter hole. The average value (obtained with circularly polarized excitation) is 5.29 dB higher than the approximate value calculated from Eq. (3.2.6) based on the Black-Hole Principle. Other data listed in Table 2.1 were obtained with linearly polarized excitation which resulted in pure LSEY modes inside the enclosure. The calculated average internal fields in this case are 3.16 to 10.6 dB greater than the Black-Hole value, depending on frequency and Q. Better agreement is obtained at 4.0 GHz than at 2.0 GHz. Furthermore, the ratio of fields for the two Q-values at 4.0 GHz is more nearly equal to 3.16 (the square root of the two Q-values). Therefore, the data in Table 2.1 seem to indicate that the conditions for the Black-Hole Principle are satisfied better at 4.0 GHz than at 2.0 GHz. The significantly different results obtained with linear and circular polarization was unexpected. Further study may lead to resolution of these questions.

For the data in Figures 2.1 and 2.3, the enclosure was excited by an external normally incident circularly polarized H-field, in order to eliminate the linear polarization associated with pure LSEY or LSEX modes. However, the calculations show that even under these conditions, the average value of Hz summed over all modes and averaged over the array of 24 field points is significantly less than the values for Hx and Hy. The ratio of Hz relative to Hx and Hy is related to the modal propagation constants for propagation along the z-direction and would remain unchanged with typical frequency-modulation stirring of say 100 KHz. It may be possible to increase the value of Hz and equalize the values of the three field components by employing a stationary mode stirrer to break up the rectangularity of the empty chamber. This may result in more random polarization characteristics with frequency mode stirring. However, the equipment under test may itself provide sufficient breakup of rectangularity.

2.3 Ratio of Wall to Volume H-Fields

The data in Figure(2.1) indicate that the average H-fields at points on the walls (wall points) are somewhat higher than at points away from the wall (volume points). This occurs although the normal component of H (Hz for the data of Figure 2.1) must be zero all along the wall. However, the two remaining components Hx, Hy for each mode must have maxima on the wall as required by the short circuit boundary condition.

Each of the modes contributing to the total fields is a periodic function of position with maxima and minima throughout the volume. The total field distribution for a given field component inside the enclosure is characterized by points of maximum total field where a large number of the significant modes combine constructively in phase, and by points of minimum total field where a large number of the significant modes are in phase opposition and combine

destructively. Note that these points are not at the same locations for all field components. For example, for the configuration shown in Figure (2.1), Hz, Ex, Ey have zeros for each mode on the wall at z = C, whereas Hx, Hy and Ez have maxima for each mode. Thus, each of the two modes shown in Figure (2.5) has maxima for Hx, Hy and Ez on the wall. However, as the field point moves away from the wall along the z-axis, the maxima for the two modes occur at different values of z. This is because the two modes have different propagation constants along the z-direction. Therefore, it seems likely that a large number of modes will add less constructively for volume points than for wall points. Using somewhat different words, it can be argued that in order to achieve maxima and minima at a wall point, conditions must be satisfied along two dimensions, whereas conditions must be satisfied along three dimensions for a volume point. These explanatory arguments indicate higher maxima and a lower minima at wall points, but indicate little about average values. However, Figure 2.1 shows higher average values.

The above discussion applies to empty chambers. However, the same conclusions apply to an enclosure containing an equipment under test (EUT) which has outer surface dimensions that are greater than a few wavelengths. In fact, according to the theory of an ideal reverberation chamber, the amplitudes of the induced currents on the surfaces of the EUT will be nearly the same as the induced currents on the wall surfaces of the reverberation chamber. Furthermore, it can be argued that the threat to which the EUT is exposed is not the fields surrounding the EUT directly, but the currents induced on the surfaces of the EUT by these fields. Therefore, it seems logical that the threat should be evaluated by measuring the currents on the walls of the reverberation chamber or on the walls of the EUT. Since wall currents are directly related to the tangential magnetic fields, B-dot probes can be employed to measure the wall currents. These probes can be calibrated on an absolute basis (see Section (4.2)).

2.4 Calculation of Correlation Widths

The frequency and spatial correlation widths were determined by using the computer program to calculate the E and H-fields in an empty enclosure. The methods described in [8] were employed. Table (2.2) lists calculated data for the Rome Laboratory Chamber with no mode stirrer present. Data are listed for frequencies ranging between 2.0 and 8.0 GHz, and for Q-values of 10,000 and 100,000. As defined in Section 3.3, FDIS is the 3 dB bandwidth and FBLH the minimum frequency for the reverberation region. DELF is the frequency difference and SP is the field point spacing employed in calculating frequency and spatial correlation widths [8]. The data indicate that the frequency correlation width designated as FCOR ranges between 51 and 100 KHz. The values of FCOR do not seem to be a strong function of the frequency or Q, or to vary in any simple way with respect to these variables. The calculated values of the spatial correlation widths (XCOR) for the Rome Laboratory Chamber range between 1.75 and 4.5 cm.

Table (2.3) lists data calculated for the Sandia chamber [8] with no mode stirrer present, and compares these with measured data (in parenthesis) for this chamber with a stationary mode stirrer present [8]. This chamber with mode stirrer has a measured Q which is nearly constant for the frequency values in Table (2.3). The calculated values of FCOR for this chamber with no mode stirrer range between 82 and 105 KHz. On the other hand, the measured values with mode stirrer present are only about 30 to 40 percent of the calculated values. Similarly, the measured values of XCOR are about 60 percent of the calculated values. It is not possible to conclude at this time that the presence of the mode stirrer is a significant reason for the difference between measured and calculated values of FCOR and XCOR. However, the values are in close enough agreement to be useful for establishing first-order requirements for frequency modulation mode stirring.

Table 2.1 Calculated Values of H-Field Magnitudes Averaged Over 24 Probes (Rome Laboratory Chamber), (Linear Polarization)

F (GHz)	Q	HMAG (AVE)	Black-Hole Values	Ratio (dB)
2.0	10,000	0.06789×10^{-3}	0.01998×10^{-3}	10.6
2.0	100,000	0.1525×10^{-3}	0.06377×10^{-3}	7.65
4.0	10,000	0.09376×10^{-3}	0.05651×10^{-3}	4.39
4.0	100,000	0.2572×10^{-3}	0.17869×10^{-3}	3.16

Table 2.2 Calculated Autocorrelation Widths
Rome Laboratory Chamber

DELF = 10.0 KHz, SP = 0.5 cm

F (GHz)	Q	FDIS (KHz)	FREV (KHz)	FCOR (KHz)	XCOR (cm)
2.0	10,000	200.0	831.0	80.0	4.5
2.0	100,000	20.0	1790.0	80.0	4.5
4.0	10,000	400.0	831.0	80.0	3.25
4.0	100,000	40.0	1790.0	51.0	2.5
6.0	10,000	600.0	831.0	100.0	3.0
6.0	100,000	60.0	1790.0	70.0	1.85
8.0	10,000	800.0	831.0	90.0	1.75
8.0	100,000	80.0	1790.0	60.0	3.0

Table 2.3 Calculated Autocorrelation Widths (Summary)
Sandia-Size Chamber (8 x 10 x 20 Feet) - (No Mode Stirrer)

DELF = 10.0 KHz, SP = 0.5 cm

F (GHz)	Q	FDIS (KHz)	FREV (KHz)	FCOR (KHz)	XCOR (cm)
2.0	20,000	100	1679.0	82.0	3.75
4.0	20,000	200	1679.0	90.0 (30.0)	3.5 (2.0)
6.0	20,000	300	1679.0	105.0 (30.0 to 40.0)	2.75 (1.7)
8.0	20,000	400	1679.0	100.0 (30.0 to 40.0)	2.5 (1.5)

Values in parentheses are average values measured by Sandia [8] with stationary mode stirrer present.

ROME LABORATORY CHAMBER

A = 3.69 METERS
B = 5.18 METERS
C = 9.78 METERS
D = 0.20 Inches

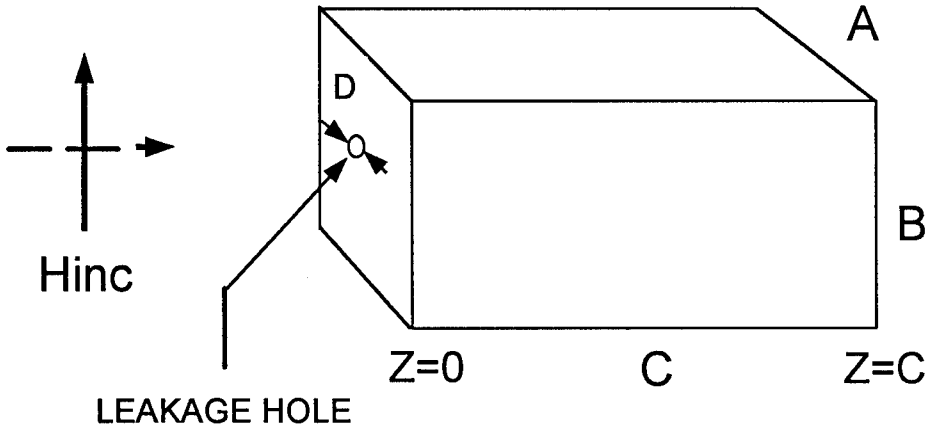

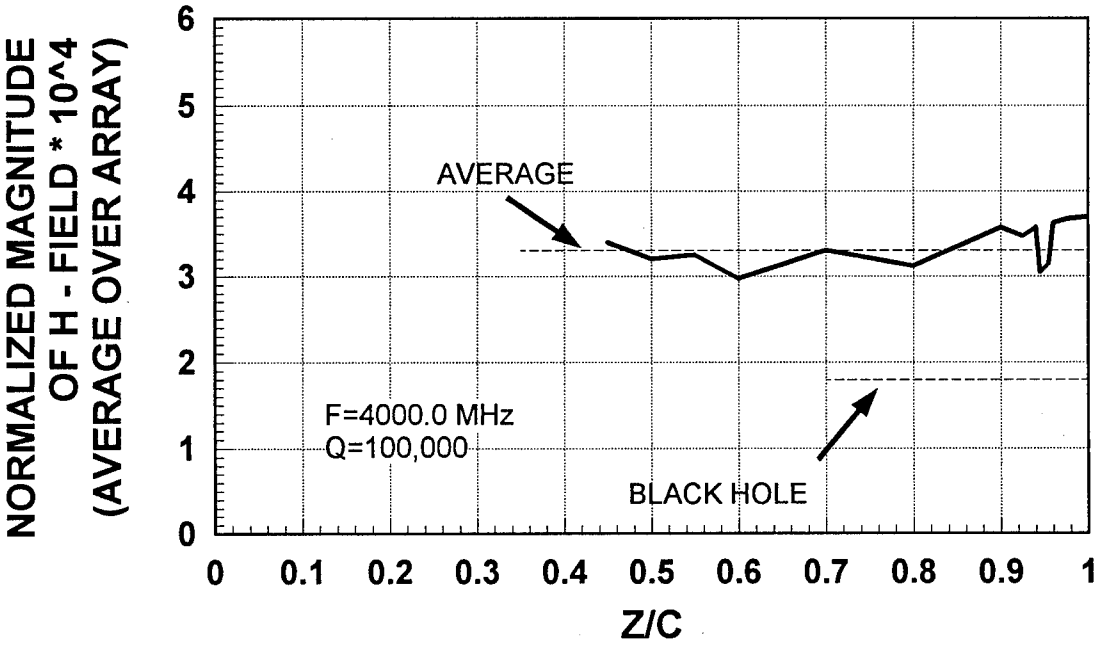

FIGURE 2.1

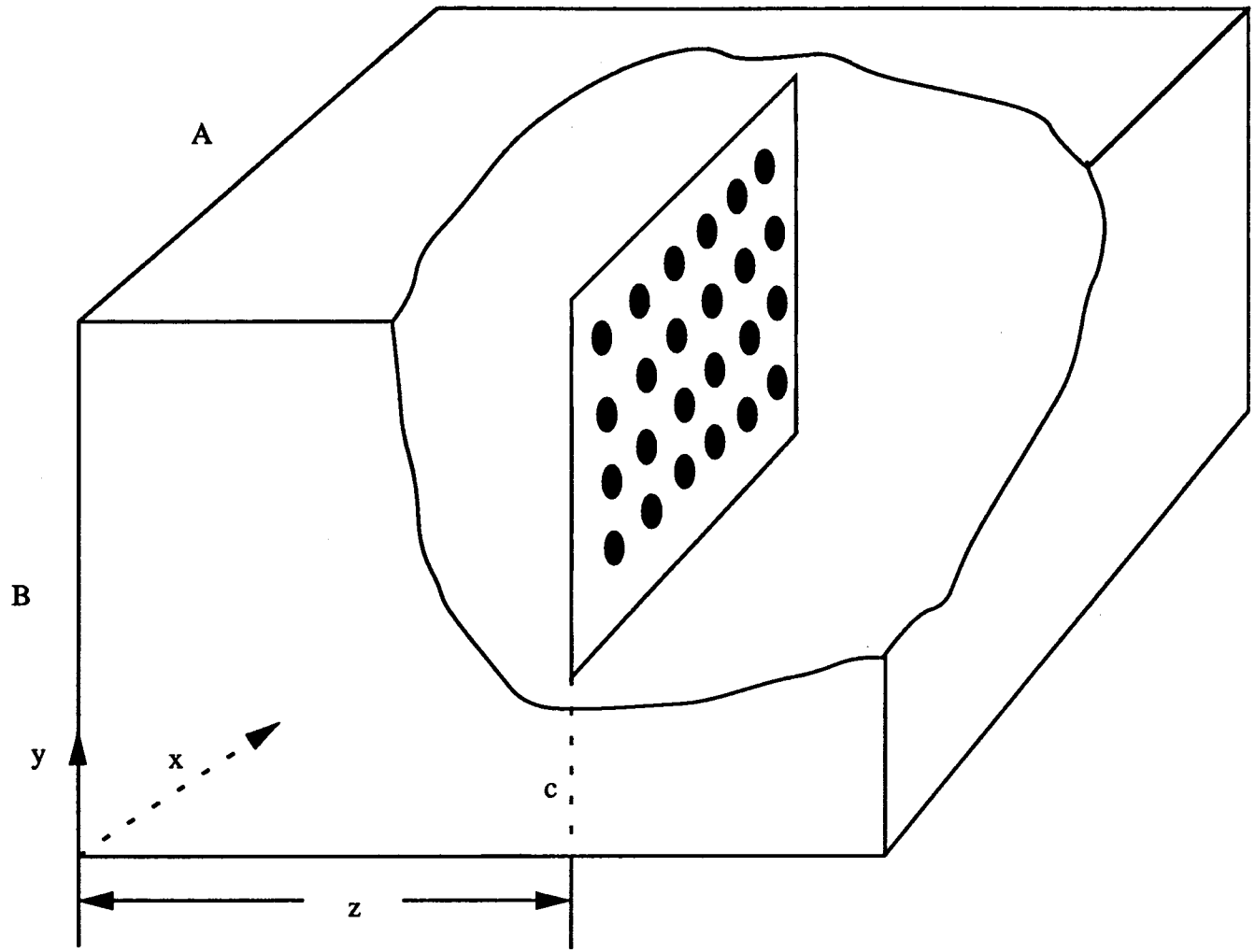

Figure 2.2 Rectangular Enclosure with Planar Array of Field Points

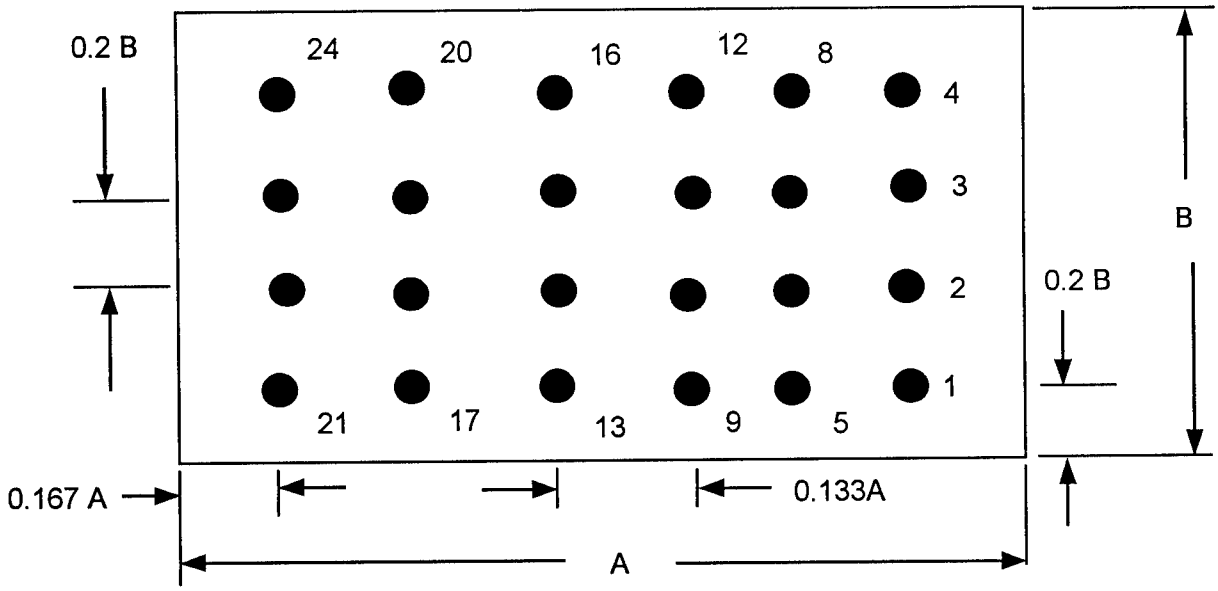

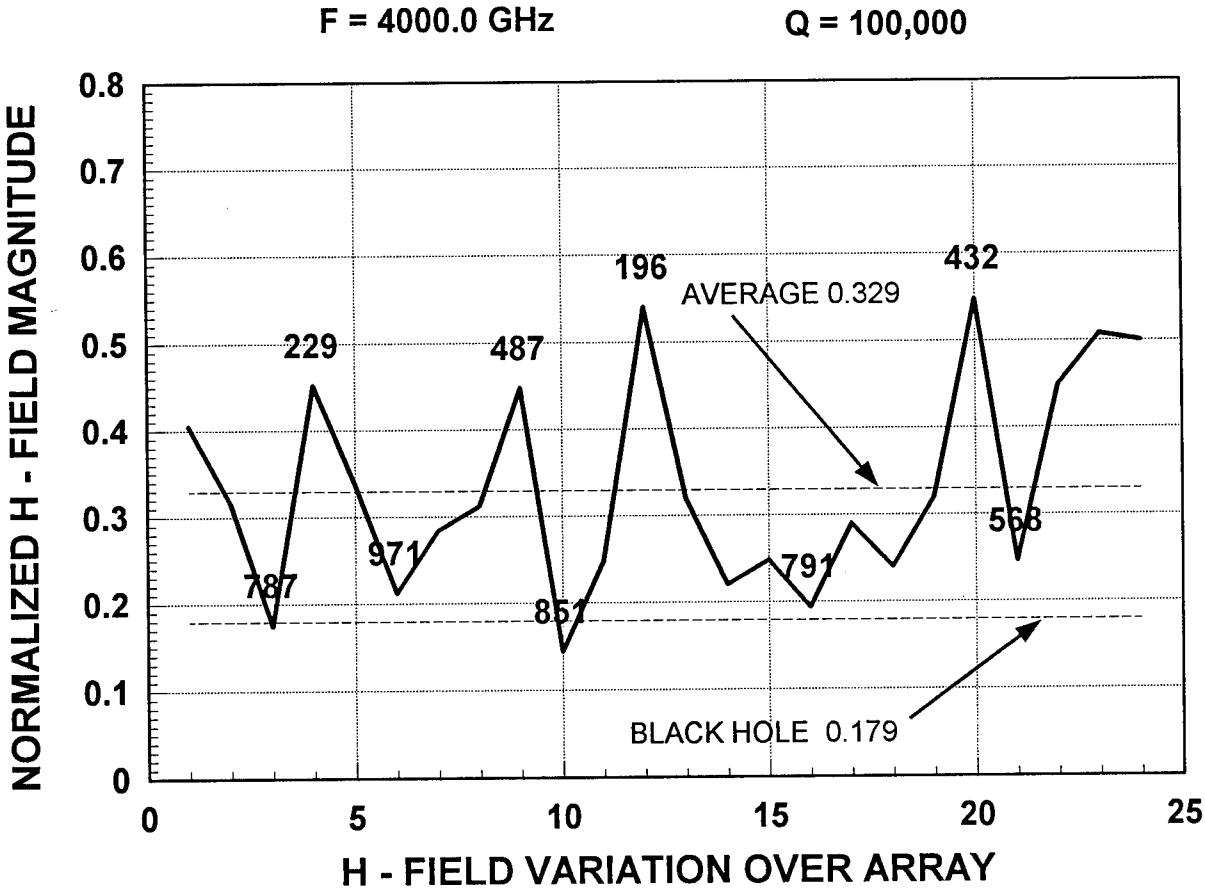

FIGURE 2.3 FIELD POINTS

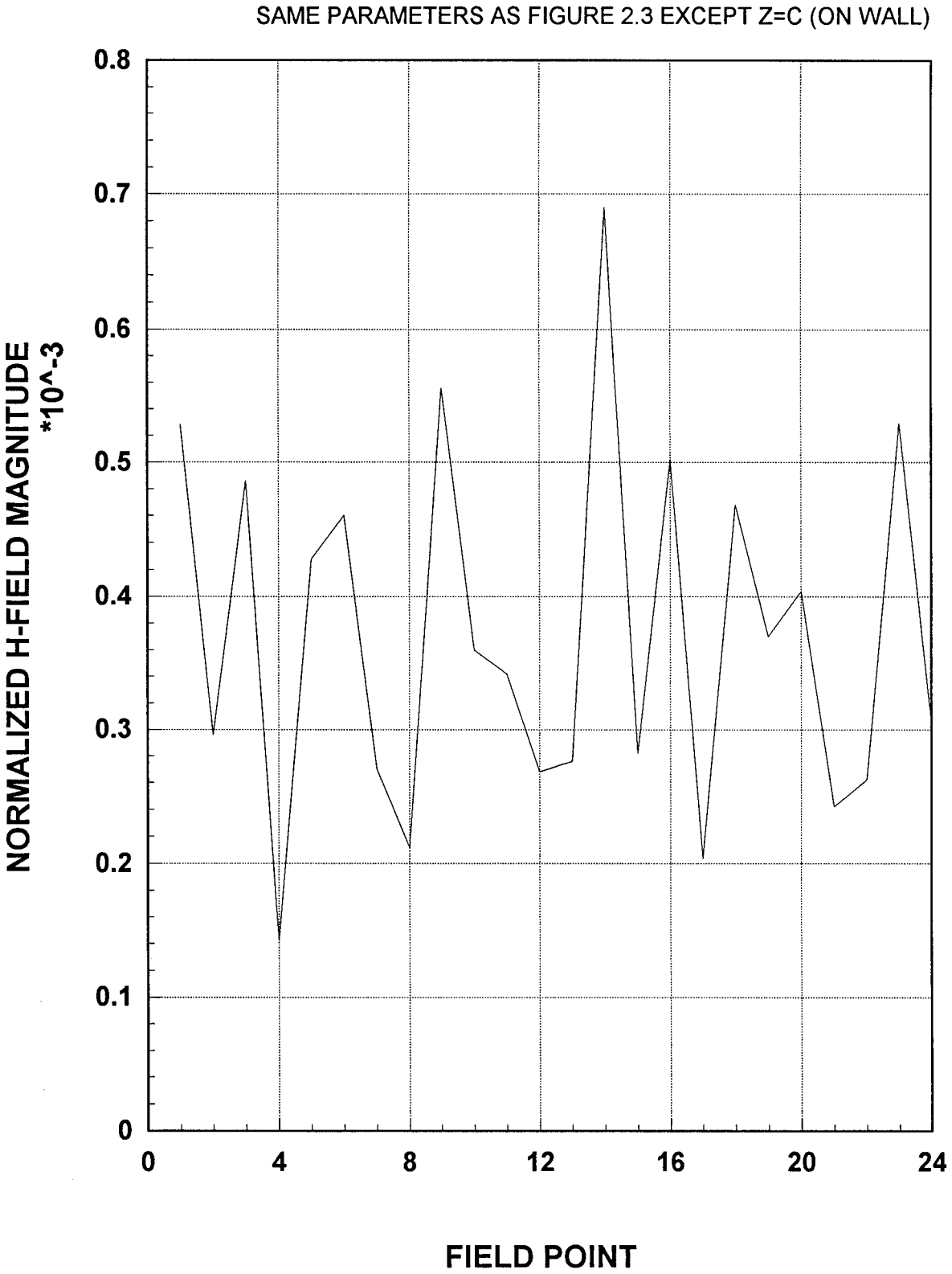
SAME PARAMETERS AS FIGURE 2.3 EXCEPT Z=C (ON WALL)
NORMALIZED H-FIELD MAGNITUDE
*10^-3
0.8
0.7
0.6
0.5
0.4
0.3
0.2
0.1
0
0
4
8
12
16
20
24
FIELD POINT

FIGURE 2.4

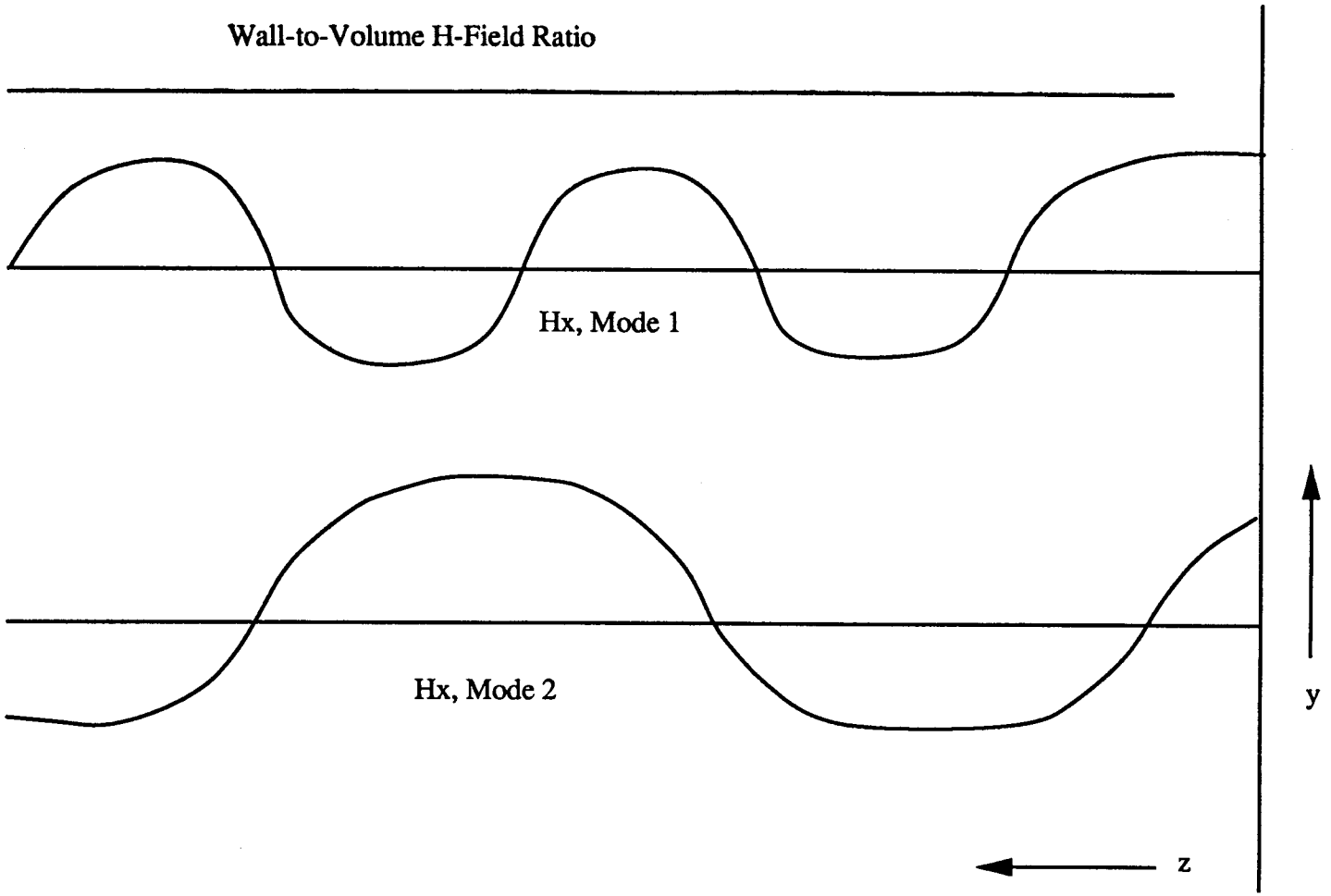

- On Surface (Hz = 0)
  Hx, Hy Always at Spatial Maxima
- In Volume
  Modal Maxima Occur at Different Points

Figure 2.5 Constructive and Destructive Combining of Modes

3.0 APPLICATION OF THE BLACK-HOLE PRINCIPLE TO REVERBERATION CHAMBER AND SHIELDING ENCLOSURES

3.1 Introduction

The Black-Hole Principle is a well known principle of physics that has been applied to the microwave region to obtain rough estimates of the shielding effectiveness of shielding enclosures. [3] In this report, it is employed to obtain rough estimates of the fields inside a reverberation chamber for comparison with the presumably more accurate calculations obtained with the computer program described in Section 2.1. Figure 3.1 illustrates this well-known principle of physics [4],[5]. Briefly, if an electromagnetic field is incident on a small hole in a wall of an enclosure, the total net power PDIS that leaks into the enclosure and is absorbed inside the enclosure can be approximated by the power PRAD that leaks through an identical hole in a wall of the same thickness and having infinite extent that separates two semi-infinite half-spaces.

For PDIS to approach PRAD, the hole size D must be fairly small relative to the enclosure dimensions, A, B, C (as in Figure 2.1). Furthermore, the enclosure dimensions A, B, C must be large compared to the wavelength λ, in order to ensure that the enclosure can support a large number of modes. It is also required that the Q for dissipation inside the enclosure be less than a certain value, depending on the size of the enclosure. The first condition that the hole size be small relative to the enclosure dimensions is usually well satisfied in a typical enclosure, and will be derived below in Section 3.2.4. A qualitative relationship between enclosure dimensions relative to wavelength for a specified Q-value will also be derived. First, however, the enclosure shielding effectiveness SE, will be derived based on the Black-Hole Principle.

3.2 Derivation of Black-Hole Principle and Shielding Effectiveness

Shielding effectiveness (SE), or preferably inverse shielding effectiveness (ISE) is defined as the ratio of the spatial average of the square of the RMS H-field, HINT inside the enclosure to the RMS value of the square of incident H-field HINC. The value of SE or ISE can be derived from the definition of Q, thus

$$Q = \frac{\omega \text{ Total Stored Energy}}{\text{PDIS}} \tag{3.2.1}$$

$$\text{Total Stored Energy} = \mu(\text{HINT})^2 VOL \tag{3.2.2}$$

$$\text{PDIS} = \eta \text{EFFA}(\text{HINC})^2 \tag{3.2.3}$$

where

$\omega = 2\pi F$

F = Frequency in Hertz

$\mu = 4\pi \times 10^{-7}$ Henries/Meter

VOL = A x B x C in cubic meters

EFFA = Effective Aperture of Leakage Hole

$$\eta = 120\,\pi \text{ ohms}$$

Equation (3.2.3) based on the Black-Hole Principle, states that PDIS is equal to the power entering the hole due to the incident power flux. Equations (3.2.1) to (3.2.3) lead to

$$\text{ISE} = \frac{1}{\text{SE}} = \left(\frac{\text{HINT}}{\text{HINC}}\right)^2 = \frac{\eta(\text{EFFA})Q}{\omega\mu VOL}$$

But, since $\eta / \omega\mu = \lambda / 2\pi$

$$\text{ISE} = (Q / 2\pi)(\lambda \text{ x EFFA} / \text{VOL}) \qquad (3.2.4)$$

For holes having all dimensions larger than about $\lambda/2$, EFFA is given approximately by the geometrical area. For round holes having diameter D less than about $\lambda/2$

$$\text{EFFA} = (8\pi^3 / 27)\, \text{D}^6 / \lambda^4 \qquad (3.2.5)$$

Substituting Eq. (3.2.5) into Eq. (3.2.4) yields

$$\text{ISE} = \left(\frac{\text{HINT}}{\text{HINC}}\right)^2 = (4\pi^2 / 27)(QD^6 / (\lambda^3\ \text{VOL}) \qquad (3.2.6)$$

Values of ISE calculated using Eq. (3.2.6) were compared to the values calculated with the computer.

3.3. Minimum Number of Modes for Validity of Black-Hole Principle

One basis that was investigated for establishing a condition for the minimum number of modes is to require that the number of modes contained within the dissipation bandwidth ΔFDIS (= F/Q) be a large number, NDIS. The total number of modes N that the enclosure can support up to a specified frequency F is given approximately by [6]

$$\text{N} = \frac{8\pi}{3}\frac{\text{VOL}}{\lambda^3} \qquad (3.2.6)$$

Figure (3.2) illustrates these relations. The value of NDIS can be determined by differentiating Eq. (3.2.6) with respect to wavelength. Thus,

$$dN = -8\pi \, \mathrm{VOL} / \lambda^3 \left(\frac{d\lambda}{\lambda} \right) = 8\pi \, \mathrm{VOL} / \lambda^3 \left(\frac{\mathrm{dF}}{\mathrm{F}} \right) \qquad (3.2.7)$$

Letting dN = 1, there results

$$\Delta\mathrm{FSEP} = \mathrm{F}\lambda^3 / 8\pi \, \mathrm{VOL} \qquad (3.2.8)$$

The bandwidth ΔFSEP is the average frequency separation between adjacent modes. The number of modes in ΔFDIS is therefore

$$\mathrm{NDIS} = \Delta\mathrm{FDIS}/\Delta\mathrm{FSEP} \qquad (3.2.9)$$

$$\mathrm{NDIS} = 8\pi\mathrm{VOL}/(\lambda^3 \mathrm{Q}) \qquad (3.2.10)$$

Solving Eq. (3.2.10) for λ^3 yields

$$\lambda\mathrm{REV}^3 = 8\pi\mathrm{VOL}/(\mathrm{NDIS\ Q}) \qquad (3.2.11)$$

$$\mathrm{FBLH} = \mathrm{C} / \lambda\mathrm{REV} = \mathrm{C} \left(\frac{\mathrm{NDIS\ Q}}{8\pi \, \mathrm{VOL}} \right)^{1/3} \qquad (3.2.12)$$

where C = 2.997925 x 10^8 M/sec is the velocity in free space.

Summarizing, Eq. (3.2.10) gives the total number of modes NDIS within the dissipation bandwidth ΔFDIS = Q/F, and Eq. (3.1.12) gives the frequency FBLH below which there are fewer than a specified required number of modes NDIS. If the required value of NDIS could be determined, then the calculated value of FBLH for given values of Q and volume may represent the minimum frequency for Black-Hole.

Tables (3.1) to (3.3) give values of NDIS calculated from measured values of Q presented in [6], [7], [10]. It should be kept in mind that the Q-values in the tables were measured for chambers with stationary mode stirrers, whereas the NDIS values were calculated from Eq. (3.2.6) by assuming an empty chamber. The lowest frequency region can be arbitrarily defined as the region in which NDIS is less than 0.5. This results in only one mode in a bandwidth equal to twice the dissipation bandwidth ΔFDIS, and corresponds to the region of well isolated resonances. As NDIS increases above 0.5, the modal resonances begin to overlap one another, and this corresponds to the region of overlapped modes. However, the overlapped modes remain uncoupled orthogonal modes. Well into the region of overlapped modes, the individual modes become indistinguishable on a spectrum analyzer. As NDIS increases even further, the Black-Hole region is entered.

The antenna VSWR data presented in Figure (2.22b) of [6] and Figure (3.1) of [7] can also be analyzed in conjunction with the values of NDIS presented in Tables 3.1 and 3.2 of the present report. A principal feature of these data as frequency is increased is the sharp drop in VSWR to the fairly low value corresponding to the VSWR of the same antenna radiating into a free-space environment. Thus, at high frequencies, the VSWR data for the three adjustments of the mode stirrer blend together and become independent of mode stirrer position. This corresponds to the condition for the validity of the Black-Hole Principle. The data in [6] indicate that a blending of the three data curves occurs somewhere in the region from 4.0 to 6.0 GHz, while the data in [7] also indicate a range between 4.0 to 6.0 GHz. Tables 3.1 to 3.3 show values of NDIS calculated from Eq. (3.2.10) that range between 25 and 59 for [6] and 26 to 75 for [7]. This indicates that a reasonable empirical value for NDIS may be about 50. Using this value for NDIS and the geometric mean of the Q values in Eq. (3.2.12), there results

$$\text{FBLH[6]} = C\left(\frac{50 \times 134.9 \times 10^{-3}}{8\pi \times 38.19}\right)^{1/3} = 5.74 \text{ GHz}$$

$$\text{FBLH[7]} = C\left(\frac{50 \times 458.26}{8\pi \times 186.94}\right)^{1/3} = 5.08 \text{ GHz}$$

$$\text{FBCH[10]} = C\left(\frac{50 \times 161.25}{8\pi \times 45.307}\right)^{1/3} = 2.672 \text{ GHz}$$

The low value for FBLH[10] results mainly from the relatively low Q-value. Based on these few examples, Eq. (3.2.12) appears to give reasonable values of FBLH using the empirical value of 50 for NDIS. Note that doubling the value assumed for NDIS would result in an increase in FBLH by a factor of 1.26. More analysis and experimental data may establish the required value of NDIS more firmly. This would be useful in estimating shielding effectiveness of an arbitrary enclosure. Data in Figure (3.8) of [7] show that with a well designed mode stirrer, random polarization is obtained above 500 MHz, which is much less than FBLH.

With regard to the presence of a mode stirrer, it can be argued that if the mode stirrer orientation has a significant effect on antenna impedance, then operation is clearly not in the Black-Hole region. It can also be argued that if the chamber is operating in this region, any object placed in the room (e.g., equipment under test) should have only an insignificant effect on the antenna impedance.

3.4 Maximum Allowable Value of Q--AND the Effective Aperture for Wall Losses

In this section, the maximum value of Q for validity of the Black-Hole Principle will be established. It is also of interest to determine the maximum hole size that will not cause a

significant reduction in Q. This issue has arisen in implementing certain methodologies for measuring shielding effectiveness of highly attenuating cover panels.

The approach is to derive an expression for the effective aperture EFFAW for wall losses. EFFAW is defined as

$$\text{EFFAW} = \frac{4(\text{PDIS})}{\eta|\text{HSURF}|^2} \tag{3.2.13}$$

where PDIS is the total power dissipated over the physical surface of the walls, and |HSURF| is the RMS H-field tangential to the surface and averaged over the total surface. The factor of 4 in the numerator converts the total tangential surface field to an incident field equal to half the total. The value of PDIS is given by

$$\text{PDIS} = \frac{\omega\mu\text{VOL}}{\eta\text{Q}} \frac{|\text{HVOL}|^2\ \text{VOL}}{\text{Q}}$$

where |HVOL| is the RMS H-field averaged over the volume. Combining Eqs. (3.2.13) and (3.2.14), there results

$$\text{EFFAW} = \frac{4\omega\mu\text{VOL}}{\eta\text{Q}} \frac{|\text{HVOL}|^2}{|\text{HSURF}|^2}$$

Since $\omega\mu / \eta = 2\pi/\lambda$

$$\text{EFFAW} = \frac{8\pi\text{VOL}}{\lambda\text{Q}} \frac{|\text{HVOL}|^2}{|\text{HSURF}|^2} \tag{3.2.15}$$

If the volume-to-surface ratio is taken as 0.5, there results

$$\text{EFFAW} = \frac{4\pi\text{VOL}}{\lambda\text{Q}} \tag{3.2.16}$$

Although Eq. (3.2.16) is based on first-order approximations and assumptions, it can provide a useful estimate of EFFAW.

The value of EFFAW given by Eq. (3.2.16) can now be compared with the effective aperture EFFA for an arbitrary size hole in the enclosure wall which radiates power back out the enclosure. Values of EFFA were given in Section (3.2.2) for practical holes. However, in

connection with the present question, holes having sizes larger than about $\lambda/2$ are of most interest, and in this case, EFFA is nearly equal to the physical area of the hole. Note that the arguments presented correctly in [6] to establish the effective aperture of an antenna inside a reverberation chamber as $\lambda^2/4\pi$ do not apply for a hole in the chamber wall.

As an example, consider a square hole of side a which is greater than $\lambda/2$. In this case, EFFA is a^2 and

$$\frac{EFFA}{EFFAW} = \frac{a^2\lambda Q}{4\pi VOL} = \left(\frac{Q}{4\pi}\right)\left(\frac{a}{\lambda}\right)^2\left(\frac{\lambda^3}{VOL}\right) \qquad (3.2.16)$$

For the chamber at Rome Laboratories,

VOL = 187 cubic meters
$Q = 10^5$
λ = 0.03m near 10 GHz

$$\frac{EFFA}{EFAW} = \frac{10^5}{4\pi}\left(\frac{27x10^{-6}}{187}\right)\left(\frac{a}{\lambda}\right)^2 = 0.001149\left(\frac{a}{\lambda}\right)^2$$

If EFFA /EFFAW is set equal to unity (corresponding to a reduction in Q by a factor of 2), $(a/\lambda)^2$ = 870 or a/λ = 29.5. Thus a 30" square opening would cause a reduction in Q by a factor of roughly 2 near 10 GHz. Equation (3.2.16) indicates that the effective aperture ratio is proportional to λ^2 for constant Q. Thus, a 60" square hole would cause a reduction in Q of roughly 2 at 5.0 GHz.

The above considerations show that holes much smaller than the above sizes do not usually play a significant role in establishing the validity of the Black-Hole Principle. However, it should be emphasized that merely having a small hole is an insufficient condition for establishing validity. The principal condition required is to have a sufficient number of modes within the dissipation bandwidth. The insufficiency of only having a small hole can be understood by noting that a very small hole can critically couple to a high-Q enclosure, in which case, the power PDIS can be much greater than the power PRAD in Figure (3.1).

Table 3.1. Calculated Values of NDIS for NIST Chamber[6]

Volume = $38.19M^3$(2.7 x 3.05 x 4.57M)

F (GHz)	FDIS (kHz)	Q	NDIS	
0.80	40.0	20.0×10^3	0.91	
1.00	33.3	30.0	1.185	Overlapping
2.00	33.3	60.0	4.74	Mode
4.00	44.4	130.0	25.3	Region
6.00	46.2	140.0	59.1	
8.00	57.1	150.0	130.0	
10.00	66.7	200.0	237.0	
12.00	60.0		307.1	Black-Hole
14.00	70.0		487.7	Region
16.00	80.0		728.0	
18.0	90.0		1036.6	
20.0	100.0		1422.0	

Reverberation Region

Table 3.2. Calculated Values of NDIS Rome Laboratory Chamber [7]

Volume = $186.94M^3$(3.69 x 5.18 x 9.78M)

F (GHz)	FDIS (kHz)	Q	NDIS	
0.10	100.0	1.0×10^3	0.17	
0.20	28.6	7.0	0.20	
0.30	15.0	20.0	0.23	
0.40	10.8	37.0	0.30	Single Insulated
0.50	7.94	63.0	0.35	Mode Region
0.60	7.50	80.0	0.47	
0.70	7.0	100.0	0.60	
0.80	6.40	125.0	0.71	
0.90	6.43	140.0	0.91	Overlapping Mode
1.00	6.67	150.0	1.20	Region
2.00	6.68	300.0	4.64	
4.00	9.52	420.0	26.52	
6.00	12.0	500.0	75.2	
8.00	13.3	600.0	148.5	
10.00	14.3	700.0	248.7	Black-Hole Region

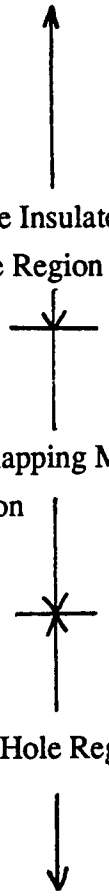

Table 3.3. Calculated Values of NDIS Sandia Chamber [10]

Volume = $45.307M^3$(2.348 x 3.0480 x 6.0960M)

F (GHz)	FDIS (kHz)	Q	NDIS
1.0	181.8	5.5×10^3	7.7
2.0	153.8	13.0	2.60
3.0	150.0	↓	56.9
4.0	200.0		135.06
6.0	300.0		263.6
7.0	350.0		455.0
8.0	400.0		723.3
9.0	450.0		1079.7
10.0	500.0		2108.7

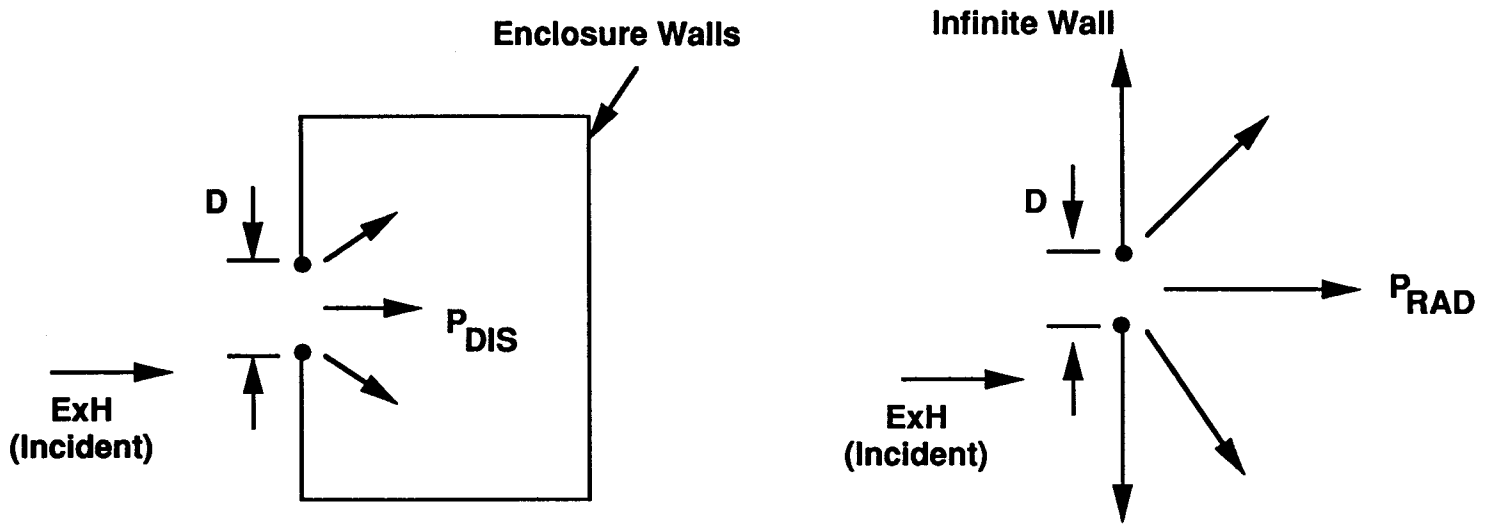

a) Opening in Enclosure

b) Opening in Infinite Wall

- **Principle: For Small Openings and Large Enclosure P_{DIS} Approaches P_{RAD}**
- **Question: Conditions of Validity**

Figure 3.1 Black-Hole Principle Illustrated

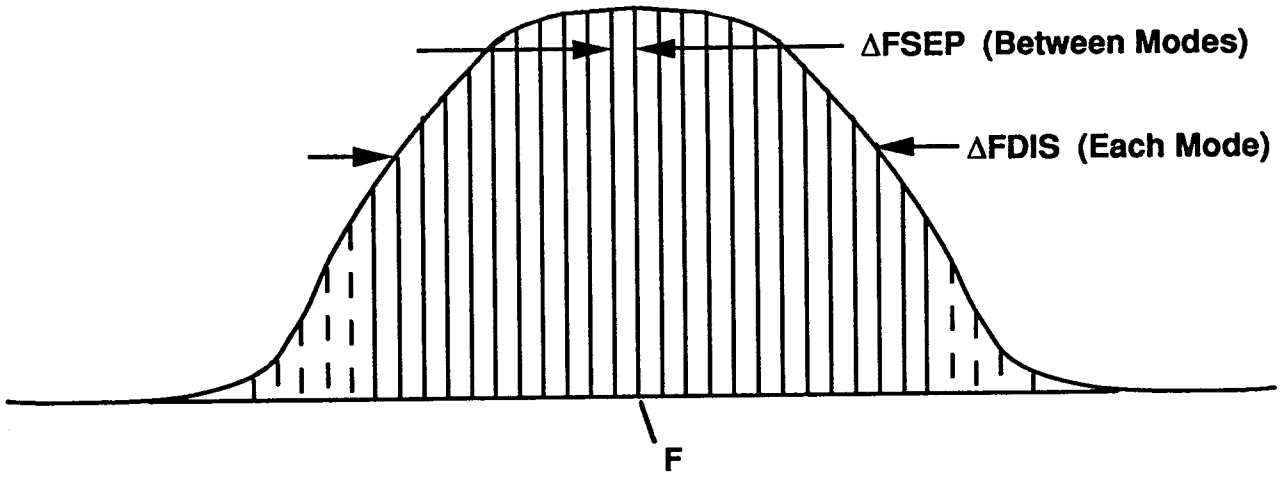

Figure 3.2 Region of Validity for Black-Hole Principle

4.0 EXPERIMENTS WITH A 30 - INCH CUBIC ENCLOSURE - FEASIBILITY OF INSERTABLE PROBES

An existing 30-inch cubic metal enclosure was employed to demonstrate the feasibility of measuring the internal fields, Q-values and the total power dissipated inside the enclosure. In particular, it was desired to demonstrate this feasibility using small probes that can be inserted from outside of the enclosure through small holes in the enclosure walls as shown in Figure (4.1). It was felt that this capability can be usefully employed to develop methodologies for measuring the shielding characteristics of Air Force equipment by non-invasive methods, that is without the need to access the interior of the equipment enclosure in order to install measurement probes.

4.1 Development of Simple B-Dot and D-Dot Probes

B-Dot and D-Dot Probes were demonstrated for "non-invasive" measurement of Q and of the E and H-fields on the internal surfaces of an enclosure. The probes are based on a simple "home-made" design, and can be inserted through existing small holes on the enclosure surface (or by removing standard lock fasteners). Data obtained from 1 to 18 GHz demonstrated that the probe readings of both E and H-fields are stable and repeatable.

Twenty randomly spaced 1/4 inch diameter holes were drilled over the area of the 1/8-inch thick top surface of the enclosure and the B-Dot probes were adjusted to seat accurately with repeatability in the holes when inserted from outside the enclosure. As shown in Figure (4.2). The probe itself consisted of a short length of 141 coaxial cable with a standard SMA bulk-head connector at the input end for connection to a coaxial line, and a modified SMA bulk-head connector on the loop end. A short metal strip 1/8" wide, 1/32" thick was soldered to the connector to form a nearly circular 0.150" diameter loop. The bulk-head connector fit snugly into the 1/4" hole and penetrated by the distance required to locate the loop appropriately relative to the inside surface of the enclosure. Probe readings were very stable and reproducible, and did not exhibit any significant "contact" effects. This good stability was obtained with both B-Dot and D-Dot probes, and represents an important finding of this development.

4.2 Probe Calibration Method

The B-Dot probes were calibrated using a network analyzer with the probes mounted on a metal plate placed at the end of a standard wave guide as shown in Figure (4.2). The metal plate exactly simulated the enclosure wall. Probe calibration factors are related to S21 measurements between wave guide input and probe cable output obtained with a network analyzer adjusted carefully for full two-port calibration. The calibration factor related the magnetic field at the probe to the voltage developed at the output connector of the probe. Measured calibration agreed very closely (within 1 dB) of theoretical calibration based on loop physical area. This calibration procedure for small probes is simpler, more convenient, and more accurate than previous methods employing standard fields produced inside anechoic chambers. It was concluded that these probes

are accurate and stable enough to be used for "non-invasive" measurement of shielding effectiveness of a given enclosure by simply inserting the probe into a small hole in the enclosure wall, and comparing the measured internal fields with measured external applied excitation fields.

4.3 Enclosure Q Measurements

The internal Q value of the enclosure was also measured using these small probes. Two methods, the transient rise/fall time method employing a fast-rise-time stepped microwave source, and the CW method in which the 3-dB width of the individual modal resonances was measured were employed. The rise time method applied for either single isolated modes or with overlapping modes, whereas the 3-dB width method can be employed only with single isolated modes. Equation 3.2.8 can be employed to calculate the average frequency separation Δ FSEP between adjacent modes. Thus, for F near 3 GHz, $\lambda = 4"$

$$\Delta \text{FSEP} = 0.283\text{MHz}$$

This should be compared to ΔFDIS = F/Q, which is about 0.3 MHz for Q = 10000. Since the value of ΔFSEP is an average value, a mixture of overlapping and nearly isolated modes can be expected. It was found that nearly equal values of Q could be obtained at several different probe positions by tuning the frequency slightly at each probe position. By tuning in this way, it was usually possible to obtain fairly good exponential time-domain wave forms at each probe position over the frequency range from 1 to 18 GHz for the 30 inch cube enclosure at a particular frequency. Values of Q calculated from measured rise time data were usually within a relative factor of 1.5 with a maximum factor of 2.0 occurring only occasionally. it should be noted that an error in Q by a factor of 1.5, would represent an error in calculated power density of 1.76 dB, and 3 dB for a factor of 2. The values of Q calculated from measured rise time data agreed with values of Q measured from measured 3-dB widths of individual modal resonance curves.

The necessity to tune the frequency slightly at each probe location to obtain a reasonable exponential wave form is only qualitatively understood at present. However, it is believed that a good exponential wave form is possible only at points of maximum field where many overlapping modes add nearly in phase. If the enclosure dimensions are large compared to a wavelength, then only a small frequency change is required to cause a maximum to occur at a given probe position.

Based on the results obtained with the insertable probes it is concluded that it is now possible to measure the absolute values of the internal fields inside a given enclosure, as well as the shielding effectiveness, and the Q-values by "non- invasive" insertable probe measurements.

4.4 Measurement of Internal Dissipated Power

The 30"-cubic enclosure was excited using a "broadband" triangular metal-strip transmitting dipole mounted in a lower corner of the enclosure. This gave reasonably low

reflections (S11 on network analyzer of - 2 dB or less) over a selected test band from 2.75 to 3.25 GHz containing 200 accurate test frequencies. It was important to carefully adjust the network analyzer for full two-port calibration.

Data was recorded for S11 and S21 (between transmitting dipole input port and probe output port) for all twenty probe locations. Data was recorded as the same probe was successfully moved from hole to hole. Both polarizations were measured. A data set for the 20 holes was obtained first with the probe oriented for one polarization, and then a second data set was obtained with the probe rotated 90°. The data for the two polarizations were nearly the same. Values of Q were also measured at several frequencies and probe locations over the test band. Equations were derived relating the total calculated wall dissipation PWALL in terms of the average magnetic fields measured at the twenty probe locations and Q values. The calculated value of PWALL normalized to the incident power PINC must equal the net power $1\text{-}S11^2$ entering the enclosure. Thus, $PWALL/PINC = 1\text{-}S11^2$.

Measurements were made with the enclosure empty, in which case the Q-values were about 33900, and with absorber placed within the enclosure to reduce the Q-value to about 3100. These Q-values were averages of values obtained at several frequencies in the test band from 2.75 to 3.25 GHz. The reduced Q was obtained by placing a small piece of absorbing material at the center of each of the four vertical side walls. The probe holes were on the top wall, and the transmitting dipole was in a lower corner of the bottom wall. After some experimentation, the right amount of absorber was determined to obtain the desired reduction in Q.

Figure 4.3 shows values of the power dissipated inside the enclosure calculated from measured magnetic field intensities and Q-values. The data are normalized relative to the net power radiated into the enclosure by the transmitting dipole antenna. Theoretically, the ratio of these two powers should be unity or zero dB. Figure 4.3 shows an average value for the two probe polarizations of about - 2.0 dB for the empty enclosure, and about - 4.5 dB for the enclosure with absorber fill.

The data for each hole position were averaged over all frequencies. This provided a smoothing of the measured H-field values to obtain an average value close to the average value that existed throughout the enclosure. Significantly, when averaged over frequency each probe was within a few dB of the correct value, indicating that a large number of probes are not required. Thus, only one or two probes with frequency averaging (frequency-modulation mode stirring) may be sufficient.

4.5 Conclusions Derived from Experiments with 30-Inch Cube Enclosure

Based on the results presented in this Section, it is concluded:

1. Insertable probes (Both B-Dot and D-Dot can be calibrated to accurately measure H and E-fields inside an enclosure.

2. Probe insertion into 0.025" diameter holes gives stable and repeatable probe output data.
3. Using these insertable probes, one can non invasively measure shielding effectiveness, Q-values and absolute values of the internal fields.
4. This non-invasive probing capability can be the basis for development of new measurement methodologies.

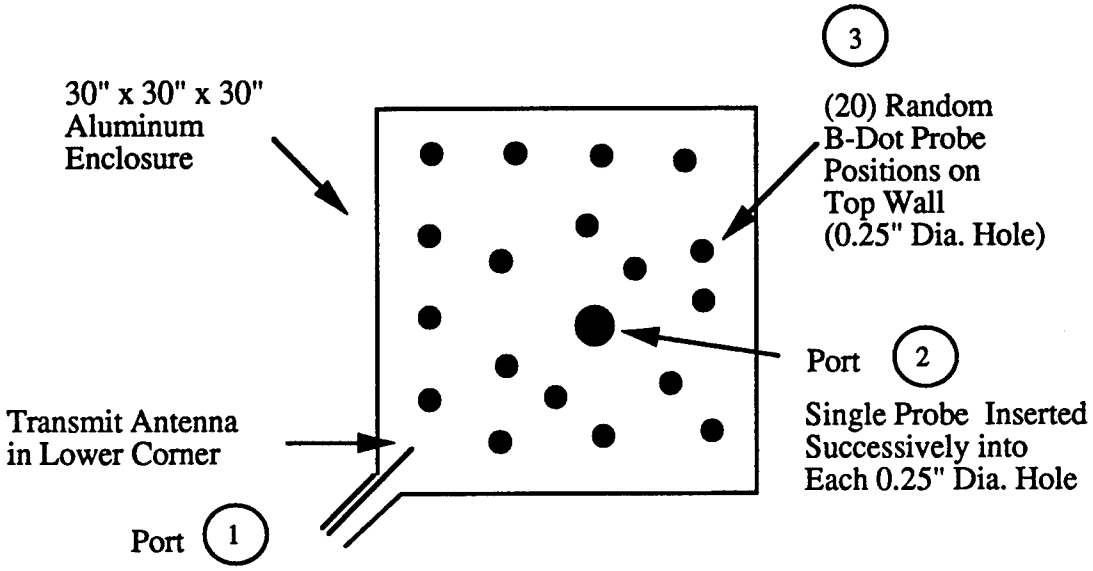

- Probes pre-calibrated by waveguide method
- Transmitter Port 1, Probe Port 2
- Measure S11, S21 with HP8510 network analyzer with full two port calibration
- Magnetic field on top wall averaged over 20 probe positions
- Measure Q through rise time
- Define:

$P_{INPUT}=1-S11_2$

$P_{DIS}=\omega\mu H_{2AVE}VOL/Q$

Figure 4.1 30-Inch Cubic Enclosure Experiment

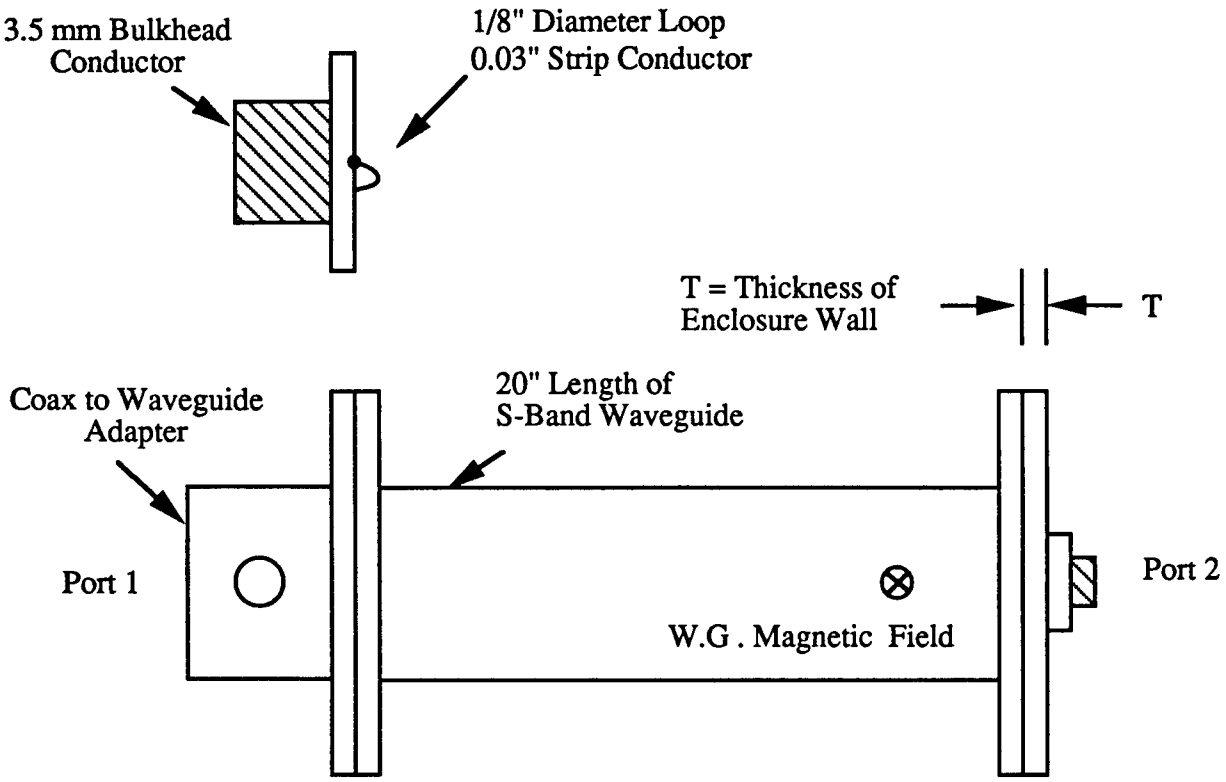

Figure 4.2 Insertable B-Dot Probe and Calibration Setup

30.0" CUBIC ENCLOSURE EXPERIMENT

(AVERAGES OVER ALL FREQUENCIES - AT EACH PROBE)

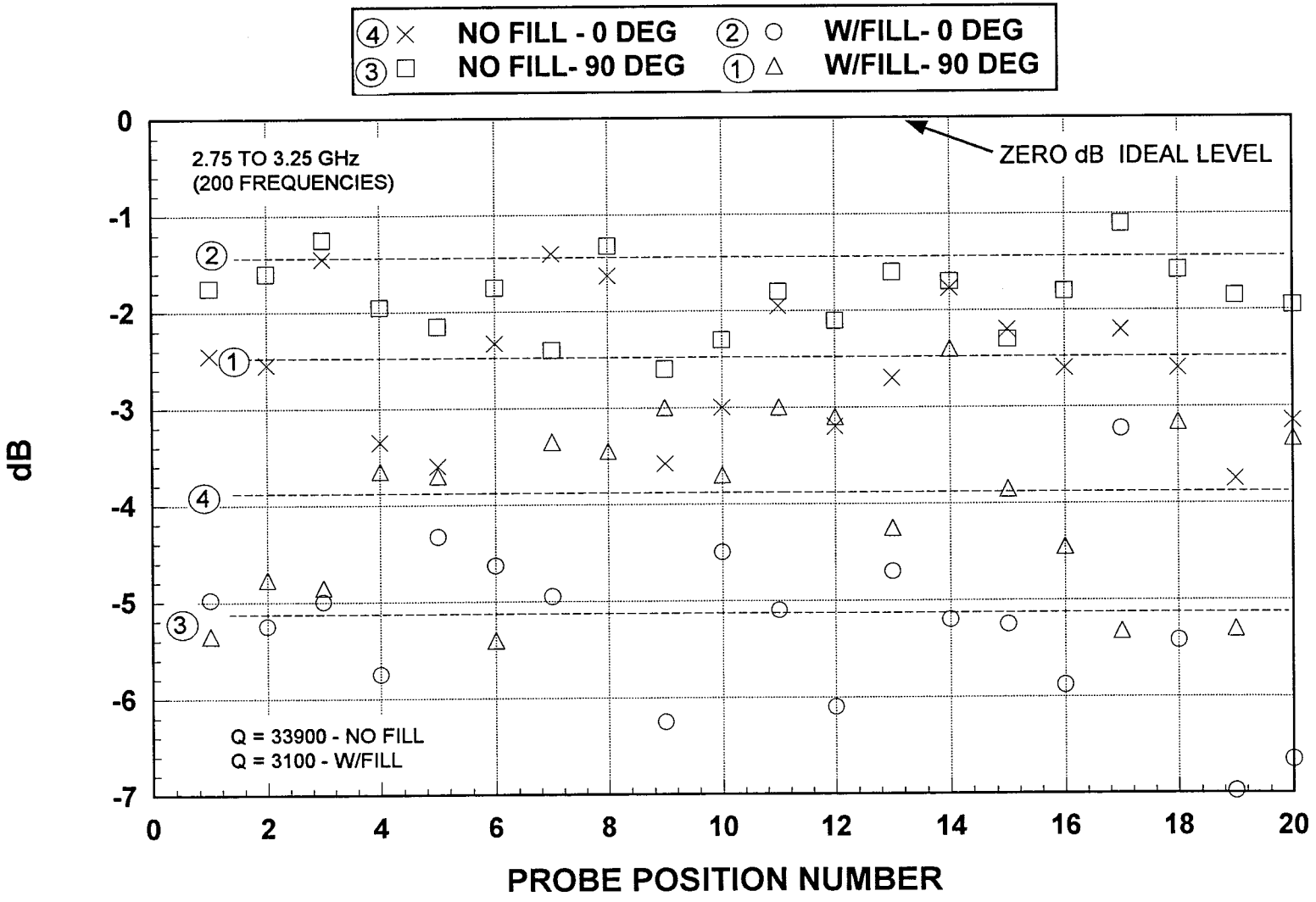

FIGURE 4.3

5.0 MEASUREMENT METHODOLOGIES

Development of measurement methodologies was one of the objectives of this program. In this section, measurement methodologies will be discussed that are based to some extent on new relationships and understanding developed on this program. Some may seem more practical than others, but all will be discussed in order to illustrate principles. On the other hand, methodologies for measuring highly attenuating cover panels and gaskets that are discussed are believed to be of significant current interest.

5.1 Methodologies Based on the Assumption that the Product SE x Q is a Constant

Equation (3.2.4), based on the Black-Hole Principle, relates inverse shielding effectiveness (ISE) to Q, EFFA and VOL. If ISE is divided by Q,

$$ISE/Q = (\lambda/2\pi)\, EFFA/VOL \qquad (5.1)$$

Thus, Eq. (5.1) shows that for a given enclosure of specified volume and set of leakage holes represented by EFFA, the ratio ISE/Q (or SE x Q) is a constant in the reverberation region.

The product of SE x Q is also a constant for a single isolated mode, provided the applied frequency F is equal to the resonant frequency, FR. However, as F moves off FR, the external fields decrease rapidly, and when F is one or two bandwidth above or below FR, the internal fields become independent of Q. Thus, the dependence on Q of a single isolated mode follows that of a single-tuned circuit. In the transition region of overlapping modes (see Section 3.3), the product of SE x Q is not a constant even if F is equal to the resonant frequency FR at a selected mode. This is because the contributions to the internal fields at F = FR of non-resonant adjacent modes are less dependent on Q than the contribution of the selected resonant mode of F = FR. The effect is to cause the value of SE to increase with decreasing Q at a rate less than 1/Q. A limited number of computer calculations indicate departures of about 3 dB for a reduction in Q by a factor of 10 (i.e., by 10 dB). Thus, SE increased by 7 dB rather than by 10 dB. More calculations of this kind may reveal more details of the transition region. It is concluded that the product SE x Q can be considered constant except within the transition region where relatively small departures from can be expected.

Figure 5.1 shows how the assumption of constant (SE x Q) can be applied to develop a measurement methodology. First, consider an empty enclosure for which SE_E and Q_E are known from measurements. Next, consider the same enclosure with the same leakage holes which has been filled with absorbing elements in the form of equipment modules to obtain SE_F and Q_F. Individually, the values for the filled enclosure are not known. However, it can be assumed that the products must satisfy the condition

$$SE_F\, Q_F = SE_E\, Q_E \qquad (5.2)$$

Thus, if either SE_F or Q_F is measured, the other can be determined if SE_E and Q_E are known. For non-invasive measurements with insertable probes as described in Section (4.1), the measurement of SE_F requires a well-calibrated probe. However, measurement of Q_F can be accomplished non-invasively with an uncalibrated probe.

A methodology based on these principles can proceed as follows. First, assume that a representative empty enclosure is available and that SE_E and Q_E are measured and recorded. The product $SE_E\, Q_E$ should be nearly equal for all empty enclosures built alike. The value of SE_F for an operational filled enclosure can then be determined by measuring Q_F. Note that if Q_F is not significantly less than Q_E, then SE_E can be taken as a pessimistic maximum value for SE_F.

5.2 Methodology Requiring No Measurements on the Filled Enclosure

In this methodology, separate measurements are made only on the empty enclosure and on the equipment modules that are intended to be placed inside the enclosure. From these data, the shielding characteristics SE_F and Q_F of the enclosure filled with the intended modules can be calculated. The empty enclosure is characterized by SE_E and Q_E, which can be measured separately. The modules can be characterized individually or collectively by an effective absorption area A. This is defined as the ratio of the total power absorbed by the module (or group of modules) divided by the effective incident power per unit area. Absorption area can be measured by the change in-Q method described below. Thus, the proposed methodology is based on the assumption that the measurement of the enclosure characteristics and the measurement of the module characteristics are separable problems.

Figure 5.2 illustrates the change-in-Q method [9] for measuring absorption area, A. Any convenient size test enclosure that need not be the same size as the intended enclosure can be employed for these measurements. The Q of the test enclosure should be as high as possible relative to that of the intended enclosure. First, the value of Q'_E of the empty test enclosure is measured and the absorption area A'_E for the interval losses can be calculated using Eq. (3.2.160. The primes indicate test enclosure.

$$A'_E = (4\pi/\lambda)\, V'_E/Q'_E \qquad (5.3)$$

where V'_E is the volume of the empty test enclosure. The modules are then placed inside the test enclosure (singly or multiply) and the Q is measured again as Q'_F. A'_F is then calculated as

$$A'_F = (4\pi/\lambda) V'_F / Q'_F \qquad (5.4)$$

where V_F' is the volume of the filled test enclosure, and is equal to V_E' minus the volume occupied by the modules. A_F' is the combined absorption area due to the test enclosure wall losses and module absorption. Therefore, the absorption area of the module A_{MOD} is given by

$$A_{MOD} = A_F' - A_E' \tag{5.5}$$

$$A_{MOD} = \frac{4\pi}{\lambda}\left[\frac{V_F'}{Q_F'} - \frac{V_E'}{Q_E'}\right] \tag{5.6}$$

Note that A_{MOD} is assumed to be the characteristic absorption area of the module, and is not primed in Eqs. (5.5) and (5.6). Thus, A_{MOD} is assumed to be independent of the test enclosure in which it is measured. If A_{MOD} is measured for each module separately, then the total value of A_{MOD} for the assembly of N modules can be assumed to be approximately equal to the sum of the values for the individual modules. The shielding effectiveness Q_F and SE_F of the intended enclosure are given by

$$Q_F = \frac{4\pi}{\lambda}(V_F / A_F) \tag{5.7}$$

where

$$A_F = A_{MOD} + 4\pi/\lambda\left(\frac{V_E}{Q_E}\right) \tag{5.8}$$

$$SE_F = SE_E\left(\frac{Q_E}{Q_F}\right) \tag{5.9}$$

Equation (5.9) is based on the assumption that the product SE x Q is a constant (see Section (5.1)). On this basis, S_F and Q_F for the filled enclosure are calculated from measured values of SF_E, Q_E of the empty enclosure, measured A_{MOD} of the individual modules, and with no measurements required on the filled enclosure.

It might be argued that the measurement of A_{MOD} by the change-in-Q method may be an insensitive method because Q_F' may not be significantly different than Q_E' . However under these conditions (which may not be uncommon in practice), the value of SE_F would also be only insignificantly less than SE_E, and in this case, this is the desired answer that has been sought. On the other hand, a significant change in Q would indicate that SE_F would be significantly greater

than SE_E. On this basis, it can be concluded that the change-in-Q method can provide a useful methodology.

The above calculations are based on Eq. (3.2.16), and there is significant uncertainty about the proportionality factor $4\pi/\lambda$. This factor was obtained by making assumptions about the ratio of wall to volume field averages and should be expressed more generally as $K(4\pi/\lambda) = K'/K$ where K' is an uncertain factor believed to be close to unity. Referring to Eqs. (5.7) and (5.8), QF should be modified to

$$Q_F = \frac{K'_{VF}}{A_{MOD} + K'V_E Q_E} \tag{5.10}$$

But Eq. (5.6) shows that A_{MOD} should be modified in the same way, with the result that Q_F is independent of K', and depends only on measured Q-values and volumes. Note that the calculated values of absorption area do depend on the value assumed for K', but the ratios of absorption areas which determine Q_F are independent of K'. The absorption areas A_E and A_F can therefore be considered as intermediate calculated parameters.

Table 5.1 lists some measured Q-values and calculated absorption areas. The enclosure employed was the small moveable reverberation chamber at Rome Laboratories, with the mode stirrer kept stationary. Subassemblies 1 and 2 were available Air Force modules that were supported on styrofoam pads when placed inside the enclosure. The 2 x 2-foot absorber was used as a "known" absorption area to check the system. It is seen that, in this case, measured values of $A_{MOD} = A_F - A_E$ compare reasonably well with the nominal area of 24 x 24 = 576 square inches. This indicates that the K'/K ratio discussed in connection with Eq. (5.10) is reasonably close to unity. Thus, the values for A_E and A_F in Table 5.1 depend on the value assumed for K', but their ratio is independent of K'. Note that only a small change in Q was obtained for module number 1, whereas a larger change was obtained for module number 2.

It has been proposed many times, by many people, over a period of many decades, that the shielding effectiveness of an enclosure can be dramatically increased by placing a small amount of low cost, low weight, low volume, absorbing material on the inside walls of the enclosure. Thus, by reducing the value of Q_E of the empty enclosure by a sufficient amount by means of absorbers, the installation of the modules would then have little effect. Under these desirable conditions, SE_F and Q_F would be nearly the same as S_E and QE, and this would remove the requirement of making any measurements at all on the filled enclosure.

A principle assumption of this methodology is that the measured value of A_{MOD} is relatively independent (within reasonable limits) of the size and shape of the test enclosure. This depends on the assumption that when the module under test is placed inside the enclosure the wall current

distribution and hence wall losses remain nearly unchanged (for a given average field in the volume). Although this is obviously a first-order approximation, it is believed that the results can provide reasonable estimates of the change in SE caused by placing equipment modules inside an enclosure.

5.3 Methodologies for Measuring Microwave Leakage Transmission Through Highly Attenuating Cover Panels and Shielding Gaskets

5.3.1 Methodologies for Measuring Microwave Leakage Transmission Thorough Highly Attenuating Shielding Cover Panels

The panel samples were fiber-loaded, and 11-inch square with thickness about one-quarter inch. Typical attenuation values ranged between 30 and 70 dB. Three methods for making these measurements were studied. These included a localized probing method in which the excitation was applied locally to small areas of the panel surface; an anechoic chamber method in which the input side of the panel was excited by a uniform plane wave, and the panel radiated into an anechoic chamber; and a reverberation chamber method in which the input side of the panel was excited by a uniform plane wave and the panel radiated into a reverberation chamber. The localized probing method will be discussed in detail, because the results obtained with this method provided insight which led to the identification of the reverberation chamber method as the optimum method.

In the localized probing method, the samples were placed between two S-band coaxial-line to-waveguide transitions (with standard wave guide plane flanges). The coaxial terminals were connected to a HP8510 network analyzer and scattering element S12 was measured as the transitions were moved along the area on opposite sides of the sample, while maintaining close alignment of the two transitions. There was no evidence of side leakage effects through the gap regions between the flanges. This can be understood by noting that the path length through the gap region is much greater than the thickness of the sample. Thus, the attenuation through the gap region is much greater than the attenuation through the sample. This is true unless the attenuation through the sample is very high as in the case of a highly conducting metal sample. In this case, the small air gaps between sample and flange may lead to leakage errors.

Although this method, when employed with unamplified power levels from the HP8510 has dynamic-range sensitivity limitations, the results obtained with the low attenuation samples (30 to 40 dB) revealed a fundamental characteristic of the panels which profoundly affect the methodology that must be employed for making the attenuation measurements. Thus, it was found that large variations in the magnitude of S12 occurred as the transitions were moved over the area of the samples. Although not recorded as data, it is also clear that large variations also occurred in the phase of S12 caused by variations in the fiber density as well as in small variations in sample thickness (variations on the order of the skin depth which may be very small in the case of highly attenuating samples).

The effect of the variations in magnitude and phase of S12 over the area of the sample becomes important if the sample is illuminated by an incident plane electromagnetic wave. In the case of normal incidence, a wave front with essentially uniform magnitude and phase is produced over the input side of the panel. However, after passing through the non-uniform panel, the wave front on the output side of the panel can have large variations in magnitude and phase over the area of the sample. Changes in the direction of the polarization can also occur. The net result is a distortion of the aperture distribution and radiation pattern on the output side of the panel. The distorted distribution can be FOURIER analyzed in principle to determine an average component as well as the amplitudes of the harmonic components. The average component will result in a radiation pattern corresponding to the opening size as in the case of the uncovered opening. If the spatial period of a particular harmonic is small compared to a free-space wavelength, the fields produced will be localized (cut off) to the region close to the aperture, and will not produce significant radiated power. If the period is greater than a free-space wavelength, the harmonic component will produce a radiation pattern that depends on the order of the harmonic and on its symmetry. Thus, some harmonics can produce radiation nulls in the direction normal to the opening, while others can produce maxima. The total radiation pattern can be unpredictable and very complex, and this precludes accurate evaluation of shielding characteristics if the panel radiates into an anechoic chamber. It is therefore concluded that an optimum method is to illuminate the panel on the input side by a uniform plane wave, with the output side radiating into a large reverberation chamber.

Based on the above considerations, it is concluded that for an attenuating cover panel, shielding can be characterized realistically in terms of a transmission area TA which can be defined as the integrated total power radiated in all directions on the output side divided by the plane wave flux density (E x H) incident on the input side.

Thus,

$$TA = \frac{\text{Total Radiated Power (watts)}}{\text{Indicent (E x H) (watts / M}^2\text{)}} \qquad (5.11)$$

Furthermore, it may be convenient to normalize TA relative to the actual geometrical area of the sample.

Some thought was also given to the question of the variation of the panel attenuation as a function of frequency for a given physical size of the panel. First, it is well established that the transmission through the uncovered opening has an effective area approximately equal to the geometrical area when both cross sectional dimensions of the uncovered opening are large compared to a free-space wavelength. It is also well established that the transmission through the

uncovered opening varies as the cube of the cross sectional dimensions when the cross sectional dimensions are small compared to a wavelength. For example, for a square opening of side S or a round hole of diameter S, the attenuation (for field strength) is proportional to $(S/\lambda)^3$. The high and low frequency transition region occurs when S/λ is about one-half.

Now consider what happens when the opening is covered by the attenuating panel. In this case, the wavelength (skin depth) inside the attenuating panel can be very small compared to the free-space wavelength, and to an observer located inside the attenuating panel, the opening appears to be very large compared to the wavelength in the absorbing medium (skin depth). However, the radiation pattern in the free-space region on the output side of the panel is always determined by the size S of the panel relative to the free-space wavelength. On this basis, it is concluded that, if there is no distortion of the aperture distribution due to non-uniform transmission over the area of the panel, then the radiation pattern of the covered opening is nearly the same as for the uncovered opening, regardless of the value of S/λ. This conclusion implies that with no distortion, the measured panel attenuation (i.e., the ratio of transmission through the uncovered and covered hole) for any value of S/λ for which S is much greater than the skin depth in the absorbing medium is nearly the same as for a hole of infinite size.

The highly attenuating panels can be expected to be also highly reflecting with a reflection coefficient approaching unity. Therefore, significant reflection anomalies are unlikely at any particular angle of incidence, and cosine (Θ), transmission dependence can be expected, where Θ is measured relative to the normal. On this basis, it is not considered necessary to excite the panel at all possible angles of the incidence as with a reverberation chamber on the input side of the panel.

5.3.2 Methodology for Measuring Microwave Leakage Transmission Through Shielding Gaskets

The study of gaskets on this program was carried out in order to identify the close similarities between a gasket seam and an attenuating panel as described in Section 5.3.1 above. First, it should be noted that an attenuating panel radiates into a free space or into an enclosure as a two-dimensional aperture antenna, whereas a gasket seam radiates as a one-dimensional line-source antenna. It should also be clear that the transmission through a gasket is affected by non-uniformities in gasket material and cross-sectional dimensional, in the same way as for panels, and that similar conclusions apply for gaskets as stated for panels in Section 5.3.1 above.

Based on these considerations, it is concluded that the concept of gasket Transfer Impedance (TI) that has been commonly employed for gaskets at low frequencies (gasket length small compared to a wavelength) cannot be applied correctly at microwave frequencies. Instead, it is proposed that the transmission through a gasket should be characterized by an equivalent transmission area, TA per unit length along the gasket

$$TA = \frac{\text{Total Radiated Power (watts)} / L}{\text{Indicent Flux (E x H) (watts} / m^2)} \qquad (5.12)$$

where L is the gasket length.

If the gasket length L is large compared to a wavelength, the equivalent one-dimensional line-source antenna representing the gasket may radiate with a distorted radiation pattern. Therefore, it is concluded that the total radiated power in Eq. (5.12) must be measured with the gasket radiating into a reverberation chamber. Furthermore, it can be argued that it is only necessary to test a gasket with normal incidence with the incident E-field polarized normal to the length of a gasket.

Table 5.1

- Cavity Volume = 1.75 x 1.41 x 1.57M = 3.874 Cubic Meters
- Empty Cavity

F (GHz)	Q_E	A_E
1.5	7255	52.04 sq. in.
4.0	13470	74.74

- Subassembly #1

F (GHz)	Q_F	A_F	$(A_F - A_E)$
1.5	6696	56.38. sq. in.	4.34 sq. in.
4.0	12297	81.87 sq. in.	7.13 sq. in.

- Subassembly #2

F (GHz)	Q_F	A_F	$(A_F - A_E)$
1.5	4140	91.20 sq. in	39.16 sq. in.
4.0	8740	115.2 sq. in.	40.45 sq. in.

- 24" x 24" Absorber

F (GHz)	Q_F	A_F	$(A_F - A_E)$
1.5	451	837 sq. in.	785 sq. in.
4.0	940	1071 sq. in.	996 sq. in.

These calculations ignore the difference in empty and filled volumes which was less than 1%. This is considerably less than the uncertainty in the measured Q-values.

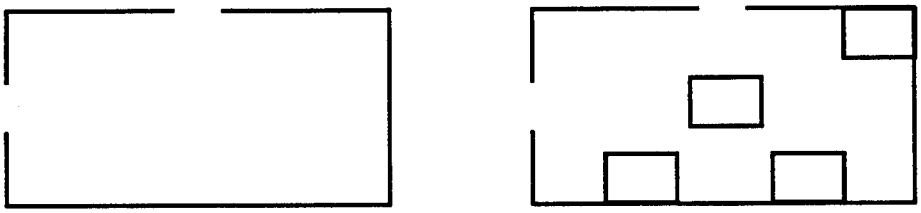

a) Empty Enclosure b) Filled Enclosure

- Measure SE and Q of empty enclosure
- Determine SE of filled enclosure by measuring only its Q-value

Figure 5.1 Methodology Based on Constant SE x Q

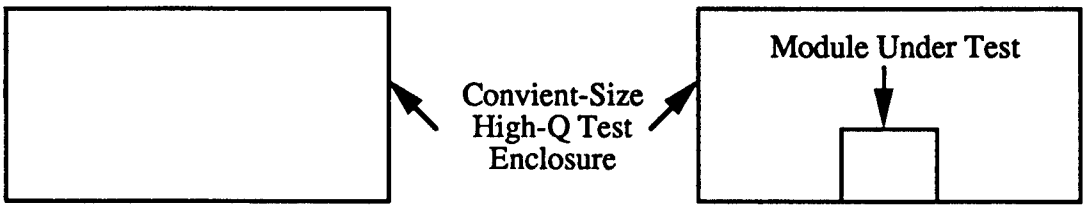

Figure 5.2 Measurement of Absorption Area of Individual Modules by Change-in-Q Method

6.0 SUMMARY AND RECOMMENDATIONS

1.0 The computer program for calculating E and H-fields inside an empty enclosure has provided results that can be useful in the study of frequency-modulated chambers. Data has been obtained on the validity of the Black-Hole Principle; on the surface-to-volume H-field ratios; on correlation widths; and on the variation of shielding effectiveness as a function of Q.

2.0 The Black-Hole Principle has been validated by comparing the power that radiates through a hole in an infinite wall in free space with the power that leaks through an identical hole in an enclosure wall and is dissipated inside the enclosure.

3.0 Three operating regions for an enclosure have been defined in terms of the number of modes, NDIS contained within the dissipation bandwidth Q/F. These are the single isolated mode region, the overlapped mode region which contains overlapping modes; and the reverberation region which contains a sufficiently large number of modes to ensure the validity of the Black-Hole Principle. The lowest frequency FBLH for this region is defined as the frequency at which the VSWR of the drive antenna becomes equal to the VSWR that this same antenna would experience in a free-space environment.

4.0 According to the concept of an ideal reverberation chamber, all components of the E and H-fields are uniformly distributed over the volume of the enclosure with equal average power densities. That is, the magnitudes of Hx^2, Hy^2, and Hz^2 must all be equal, not at each point, but when averaged over the volume. Maxima and minima occur throughout the volume at points which are different in general for each component. As a well designed mechanical mode stirrer is rotated, the points of maxima and minima for each component shift to different positions randomly, and create a condition of nearly equal average power density with random polarization (equivalent angle of incidence) at each point in the volume. The data shown in Figure (3.8) of [7] show that this performance is approached reasonably well for frequencies above about 500 MHz. However, the computer calculations show that a frequency modulated empty chamber with perfect rectangularity that is excited only on one end wall ($z = 0$) with circular polarization will experience a longitudinal component, Hz that is significantly less than the transverse components Hx and Hy. It may be possible to achieve more equal average energy density in all field components by employing corner excitation, or a stationary mode stirrer of optimum design to break up the rectangularity. Such measures may be necessary if the performance of a practical frequency-modulated chamber is to approach the performance of a well designed mechanically mode stirred chamber.

The estimated value of FBLH defined above for an empty chamber may be too high for a practical chamber with fill. Studies should be aimed at developing new methods for reducing this frequency limit for frequency modulated chambers (e.g., with fixed mode stirrers).

5. Serious consideration should be given to the proposal presented in Section (2.3) for evaluating a threat on an EUT by measuring the fields on the surfaces of the EUT or on the walls of the chamber by means of calibrated probes.

6. The feasibility of insertable probes was demonstrated by the results in Section (4.0). These probes can be important in implementing practical measurement methodologies.

7. The variation of SE as a function of Q was discussed in Section (5.1). It was shown that the produce SE x Q is a constant as a function of 0 in the region of single isolated modes only if the applied frequency is equal to the resonant frequency of the isolated mode. It was also shown that SE x Q is a constant as a function of Q above the frequency FBLH, but can deviate from a constant value by a few dB in the region of overlapping modes. Experimental studies are suggested to further explore this important question.

8. Careful experiments should be performed to determine measured values for the correlation widths of an empty chamber, and the effect of fill (e.g., stationary mode stirrer, EUT) on the measured values.

9. Important conclusions were developed considering methodologies for measuring shielding characteristics of highly attenuating cover panels and shielding gaskets. Chief among these was the conclusion that the panel or gasket under test must radiate into a large reverberation chamber in order to accurately measure the total leakage power. This is a necessary requirement because of the unpredictable highly distorted radiation pattern that results from the non-uniform transmission that occurs over the area of this panel and along the length of the gasket. Another important conclusion is that the characterization of a gasket in terms of Transfer Impedance, as is the current practice, can be meaningless at microwave frequencies. Instead, it is proposed that a gasket be characterized in terms of an equivalent transmission area TA per unit length.

10. Arguments were also presented relative to the variation as a function of frequency of the ratio of covered to uncovered transmission through an opening. It is concluded that this ratio is essentially independent of the size of the hole relative to the free space wavelength. This conclusion should be tested experimentally. If found to be correct, greatly simplified test requirements would be possible. Thus, leakage transmission through a specified uncovered hole can first be calculated with reliable established methods as a function of frequency. Then the reduction in leakage transmission would be essentially the same for all whole sizes at a particular frequency.

7.0 PUBLICATIONS AND PRESENTATIONS

1.0 J.P. Quine, K.E. Larson, W. Quinn, J.P. Streeter, J.A. Pesta, P. Fanelli, C. Blank, "Measurement of Total Absorption Area of Electronic Subassemblies", 1993 International EMC Symposium, August 17-21, 1992, Poster Session, Anaheim, CA

2.0 J.P. Quine, E.A. Surowiec, J.P. Streeter, A.J. Pesta, "Electromagnetic Studies at Rome Laboratories", presentation at Anechoic Chamber and Reverberation Chamber Operators Group Meeting at Naval Surface Warfare Center, Dahlgren Division, Dahlgren, VA

3.0 J.P. Quine, "Characterization and Testing of Shielding Gaskets at Microwave Frequencies" and J.P. Quine, "Opening Leakage of Shielded Enclosures at Low and High Frequencies". Both of these papers were accepted for presentation at 1993 IEEE International Symposium on Electromagnetic Compatibility, August 9-13, 1993, Dallas, TX

8.0 REFERENCES

[1] R.E. Collin, "Field Theory of Guided Waves", Second Edition, IEEE Press, New York, New York, 1991

[2] D.M. Pozar, "Microwave Engineering", Addison-Wesley, New York, New York, 1990

[3] J.P. Quine, "Application of the Optical Black-Hole Principle to the Estimation of Shielding Effectiveness to Radio Frequency Energy", 1989 IEEE National Symposium on Electromagnetic Compatibility, Denver, CO, May 23-25, 1989, pp. 33-35

[4] F.W. Sears, "Principles of Physics" Vol. I, Mechanics, Addison-Wesley, Inc., Cambridge, 1944, pp. 384-386.

[5] F.W. Sears, "Principles of Physics", Vol. III, Optics, Addison-Wesley Press Inc., Cambridge, MA, 1945, pp. 265-266

[6] M.L. Crawford, G.H. Koepke", Design, Evaluation, and Use of a Reverberation Chamber for Performing Electromagnetic Susceptibility/Vulnerability Measurements", NBS Technical Note 1092, April 1986

[7] M.L. Crawford, G.H. Koepke, J.M. Ladbury, "EMR Test Facilities Evaluation of Reverberation Chamber Located at RADC, Griffiss AFB Rome, New York, NBSIR 87-3080, Dec. 1987

[8] Bill Bovarie, "Mode-Stirred Chamber Field Statistics: Correlation Widths", Sandia National Laboratory, Presented at Reverberation Chamber User's Group Meeting, Boulder, CO, August 1-2, 1991

[9] C.H. Townes, A.L. Schawlow, "Microwave Spectroscopy" McGraw-Hill, 1955, pp. 439-441

[10] J.G. Kostas, B. Bovarie, "Statistical Model for a Mode-Stirred Chamber", IEEE Trans. on Electromagnetic Compatibility, Vol. 33, No. 4, November 1991, pp. 366-370

*U.S. GOVERNMENT PRINTING OFFICE: 1996-710-126-20181

MISSION

OF

ROME LABORATORY

Mission. The mission of Rome Laboratory is to advance the science and technologies of command, control, communications and intelligence and to transition them into systems to meet customer needs. To achieve this, Rome Lab:

a. Conducts vigorous research, development and test programs in all applicable technologies;

b. Transitions technology to current and future systems to improve operational capability, readiness, and supportability;

c. Provides a full range of technical support to Air Force Materiel Command product centers and other Air Force organizations;

d. Promotes transfer of technology to the private sector;

e. Maintains leading edge technological expertise in the areas of surveillance, communications, command and control, intelligence, reliability science, electro-magnetic technology, photonics, signal processing, and computational science.

The thrust areas of technical competence include: Surveillance, Communications, Command and Control, Intelligence, Signal Processing, Computer Science and Technology, Electromagnetic Technology, Photonics and Reliability Sciences.